Neuronal and Network-based Mechanisms of Spontaneous Synchronous Activity in the Developing Mouse Cortex

Heather Barnett

A dissertation

submitted in partial fulfillment of the

requirements for the degree of

Doctor of Philosophy

University of Washington

2014

Reading Committee:

Adrienne Fairhall, Chair

William Moody

Frederick Martin Rieke

Program Authorized to Offer Degree:

Neurobiology and Behavior

Abstract

Neuronal and Network-based Mechanisms of Spontaneous Synchronous Activity in the Developing Mouse Cortex

Heather Barnett

Chair of the Supervisory Committee:
Adrienne Fairhall, Associate Professor
Physiology and Biophysics

Spontaneous synchronous activity (SSA) that propagates as electrical waves is found in numerous CNS structures and is critical for normal development, but the mechanisms of generation of such activity are not clear. In previous work, we showed that the ventrolateral piriform cortex is uniquely able to initiate SSA in contrast to the dorsal neocortex which participates in but does not initiate SSA. In this study we used Ca^{2+} imaging of cultured E18-P2 coronal slices (E17 + 1-4 days in culture) of the mouse cortex to investigate the different activity patterns of individual neurons in these regions. In the piriform cortex where SSA is initiated, a higher proportion of neurons were active asynchronously between waves in comparison to the dorsal cortex. In addition, a larger number of groups of co-active cells were present in the ventral cortex than in the dorsal cortex. When we applied GABA and glutamate synaptic antagonists, asynchronous activity and cellular clusters remained while synchronous activity was eliminated, indicating that asynchronous activity is a result of cell-intrinsic properties that differ between these regions. To test the hypothesis that higher levels of cell-autonomous activity in the piriform cortex underlie its ability to initiate waves, we constructed a conductance-based network model in which three layers differed only in the proportion of neurons able to

intrinsically generate bursting behavior. Simulations using this model demonstrated that a gradient of intrinsic excitability was sufficient to produce directionally propagating waves that replicated key experimental features, indicating that the higher level of cell-intrinsic activity in the piriform cortex may provide a substrate for SSA generation.

TABLE OF CONTENTS

List of Figures ii

List of Tables iii

Introduction 1

Chapter 1 10

Chapter 2 31

Conclusions 48

References 53

FIGURES LIST

Figure 1: Asynchronous activity of individual cells and clusters in the ventral piriform cortex 16

Figure 2: Comparison of single-cell asynchronous activity in the ventral and dorsal cortex 19

Figure 3: Effects of synaptic isolation on synchronous and asynchronous activity in the ventral and dorsal cortex 22

Figure 4: Activation of a cellular cluster 23

Figure 5: Distribution of cluster size 23

Figure 6: Activation of a cellular cluster triggered by an 'off' cell 24

Figure 7: Overlap of cell participation in clusters 25

Figure 8: Spatial distribution of cellular clusters in the ventral and dorsal cortex 25

Figure 9: Effects of voltage-gated ion channel antagonists on synchronous and asynchronous activity.....26

Figure 10: Frequency of excitatory postsynaptic potentials in the ventral and dorsal cortex 28

Figure 11: Network model design and simulation.....37

Figure 12: Examples of waves in different network implementations 39

Figure 13: Persistence of activity in the ventral piriform cortex at the termination of a propagating wave 41

Figure 14: Participation in waves by layer and proportion of autonomously active cells 43

Figure 15: Duration of waves for different proportions of autonomously active neurons 45

TABLES LIST

Table 1: Asynchronous and synchronous event properties.....18

INTRODUCTION

In many regions of the developing mammalian central nervous system, spontaneous electrical activity that synchronizes large groups of neurons independent of sensory stimulation plays a critical role in development (Moody and Bosma 2005, for review). Such activity has been observed in the retina (Meister et al, 1991), spinal cord (O'Donovan et al. 1998), hindbrain (Gust et al. 2003), hippocampus (Ben-Ari et al. 1989), and cerebral cortex (Corlew et al. 2004).

The observation of SSA in diverse regions and various mammalian and non-mammalian species reveals its fundamental importance in the development of the central nervous system. The elimination of SSA in specific systems results in significant abnormalities in the mature animal. In the retina, for example, SSA is critical in the formation of functional circuitry within the retina and in downstream targets in the visual system. When activity is blocked with tetrodotoxin (TTX) during the period of synchronous waves, retinal ganglion cell (RGC) axons do not segregate into eye-specific layers in the lateral genticulate nucleus (LGN) but instead remain intermingled (Shatz et al. 1988). In V1, blocking SSA prevents the formation of ocular dominance columns. In addition, the loss of SSA results in abnormal retinotopic maps with oversized receptive fields of V1 cells (Huberman et al. 2006; Cang et al. 2005).

Synaptic plasticity may provide the general mechanism through which SSA exerts its effects. For example, it is theorized that the development of eye-specific layers in the LGN is dependent on the temporal structure of waves through a competitive mechanism of synaptic strengthening. According to this proposal, synapses onto a given target neuron in LGN compete with each other to remain present. Synapses that are active together cooperatively strengthen one another while synapses that are inactive during collective activity are weakened. Because of the relatively low frequency of waves and the shifting boundaries, it is unlikely that any two given

neurons from opposite eyes would be correlated in the timing of their activity. Only neurons close to each other on a single retina are likely to have correlated activity. This provides a explanation not only for eye-specific layers and ocular dominance columns but also the refinement of the retinotopic map and receptive fields. If only cells near each other are active in synchrony, inputs from the same retinal area will be strengthened together in higher visual processing areas, leading to patterned anatomical structuring.

In the cerebral cortex, the effects of SSA on development are under continuing investigation and appear to be widespread. SSA affects the generation, survival, and differentiation of neurons in the cortex. GABAergic interneurons are particularly affected by the patterns of synchrony during early development, and the effects are specific to certain periods of development and types of interneurons. When neurons are maintained in dissociated culture, blocking SSA with TTX during the first week *in vitro* increases the neurogenesis of small calretinin-positive GABAergic cells (de Lima et al. 2007). Thus, SSA appears to initially inhibit the proliferation of certain varieties of interneurons. During the second week *in vitro*, the role of SSA changes. SSA during this period enhances the survival of GABAergic interneurons. When SSA is blocked during this later time period, the density of small GABAergic neurons decreases and those remaining show underdeveloped morphology, indicating that activity promotes survival and differentiation in interneurons (de Lima et al. 2004). By stimulating activity in immature neurons, SSA may trigger particular genetic programs that further the maturation of these cells and promote their survival. As in the retina, coincident activity is predicted to strengthen synapses, which enhances neuronal survival.

SSA induces significant synaptic changes in the cortex that may structure communication within the network in addition to affecting maturational changes in individual

cells. Before wave activity is observed in the cortex, many glutamatergic synapses are physiologically silent due to the absence of AMPA receptors. These synapses originally contain only NMDA receptors and are therefore not active at resting membrane potential; however, when the neurons experience simultaneous presynaptic and postsynaptic depolarization, AMPA receptors are inserted into the membrane and the synapses become functional. The synchronous activation of many cells during cortical waves induces this process on a large scale across the cortex (Voigt et al. 2005). This global activation of synapses provides a substrate of network connectivity that can be refined when sensory input begins to guide neural development. In addition to the activation of glutamatergic synapses, GABAergic synapses increase in number during the period of SSA and become morphologically mature (Kato-Negishi et al. 2004). Thus, changes in synaptic transmission are a major effect of cortical SSA, and these changes provide the framework for further network maturation as the animal begins to interact with its environment.

Although waves of SSA have been observed in the cerebral cortex and are critical for development, few details are known about the mechanisms behind these waves. Intrinsic cellular properties and network architecture unique to early development may allow this phenomenon to occur during a restricted period. Certain features of immature cells, including a high resistance of the resting cell membrane and prominent low-threshold calcium currents, may enhance excitability in neurons which receive little afferent sensory input. Network properties, including an excitatory effect of GABA and the presence of gap junctions, may permit the propagation of waves of electrical activity. The mechanisms by which such properties interact to produce spontaneous synchronous activity (SSA) is a critical area of open investigation that will further our understanding of neural development.

SSA in the cortex was first described by Corlew et al. (2004) in the perinatal mouse. These waves reach peak frequency of approximately one per minute on the day of birth (P0) and decrease in frequency over the first week after birth. SSA is not observed after P10 (Conhaim et al 2011). Each wave lasts 5 to 15 seconds and involves an average of 52% of imaged neurons. As in other systems, SSA is blocked by the application of tetrodotoxin, a voltage-gated sodium channel blocker, indicating that propagation depends on action potentials generated by the immature cells which lead to neurotransmitter release (Corlew et al. 2004).

There are several unique features in the patterns of SSA in the cortex that make it an ideal system for investigating the mechanisms by which spontaneous synchrony among neurons can be initiated and propagated. In the cerebral cortex, waves of SSA originate within a well-defined spatial region in the ventrolateral piriform cortex (Lischalk et al. 2009), in contrast to systems such as the retina in which activity initiates with equal probability throughout the structure (Meister et al. 1991). In imaging experiments, 99% of observed synchronous activity in the cerebral cortex is initiated within this region. Moreover, when the region is surgically isolated from cortical slices, SSA continues to be generated within the isolated region, but SSA is eliminated in other parts of the cortex, suggesting that the ventrolateral piriform cortex is uniquely able to generate SSA and does so without input from other cortical regions (Lischalk et al. 2009). In up to 50% of ventral waves, cortical waves beginning in the ventrolateral region are preceded by activity in the septal nuclei, indicating that subcortical activity may trigger cortical waves in some cases. Surgical dissection of the connection between the septal nuclei and ventraolateral cortex demonstrated that both regions are independently able to generate synchrony (Conhaim et al 2010). In contrast, the dorsal neocortex does not generate SSA. The existence of a specific cortical region with the ability to generate SSA allows us to determine

how its properties differ from the surrounding tissue and how such properties relate to the generation of SSA. By investigating the unique properties of a region which initiates SSA, we hope to gain a more general understanding of what critical conditions are required for synchronous activity generation in a general context.

In addition to the regionalization of SSA generation that characterizes the spatial dynamics of the system, SSA in the cortex follows a temporal pattern in which the transmitter dependence of synchrony changes between early (E18 – P2) and late (P6 – P10) stages of wave propagation. During the early period when wave frequency reaches its peak, propagation depends primarily on GABAergic transmission. When picrotoxin, a $GABA_A$ receptor antagonist, is applied to cortical slices between E18 and P0, waves are blocked by more than 90%. At P6, however, picrotoxin is only 33% effective in blocking waves. At P7 it increases the frequency of waves, and by P10 it is able to induce waves when none are present in the control condition. Thus, the action of GABA on synchrony is reversed over the course of the first two postnatal weeks.

The role of glutamatergic synaptic transmission in SSA becomes more prominent over this same time period. At E18, CNQX, an AMPA receptor antagonist, reduces the frequency by only 21%; after P6, CNQX is completely effective in blocking waves. During this period, the spatial properties of SSA are also undergoing a shift. During the early stages, many waves initiated in the ventral cortex stop their propagation at the rhinal fissure. Less than 20% of waves propagate into the dorsal cortex. By P8, most waves (72%) propagate into the dorsal cortex, although waves are still initiated by the pacemaker region (Conhaim et al 2011). Thus, the features of synaptic transmission appear to play a critical role in the patterns of SSA generation in the cortex.

A possible mechanism for the change in the role of GABAergic transmission is the transition in the action of GABA from excitatory to inhibitory. Between E16 and P16 in the rat, the reversal potential for GABA in neocortical cells falls from -40 to -66 mV. This shift is due to change in the concentration of intracellular chloride (Owens et al 1996). The chloride gradient across the cell membrane is regulated by a balance of NKCC1, the Na^{+}-K^{+}-$2Cl^{-}$ transporter which controls Cl^{-} uptake, and KCC2, a K^{+}-Cl^{-} transporter that extrudes Cl^{-}. During early development, KCC2 is not expressed, leading to a relative increase in intracellular Cl^{-} and thus a more positive reversal potential for GABA. Between P0 and P15, there is a dramatic up-regulation in the expression of KCC2, which was shown to cause the developmental switch in GABA action (Rivera et al. 1999) This developmental transition in GABA action and its correlation with a shift in network behavior suggest that the mechanism terminating SSA may include the transition from a purely excitatory to a mixed inhibitory and excitatory network. Thus, network properties and communication among neurons may influence the generation and termination of SSA.

Further investigations into the nature of the GABAergic contribution to SSA revealed that the spatial distribution of GABAergic neurons is highly correlated with the region of wave initiation. When cortical slices are stain via immunohistochemistry for glutamic acid decarboxylase (GAD65/67), the enzyme that catalyzes the terminal step in the synthesis of GABA, the stain is most prominent in the septal nuclei and in the ventrolateral region. A dramatic decrease in staining occurs at the rhinal fissure where waves of SSA either pause or stop (Conhaim et al. 2011). Experiments in cell culture demonstrate that cultures from the ventral region containing large GABAergic interneurons produce spontaneous network events but dorsal

cultures do not (Baltz et al. 2010). These findings suggest that GABAergic neurons may be uniquely involved in the generation of waves of SSA.

In addition to changes in synaptic communication and network structure, the intrinsic properties of individual neurons mature over the period during which SSA occurs. Both the profile of ion channel expression in cortical neurons and their activity patterns undergo dramatic development over the first few postnatal weeks. Cortical neurons during the embryonic period have a high membrane resistance and low magnitude sodium and potassium currents. As neurons mature, they develop a lower membrane resistance, a higher membrane capacitance, larger voltaged-gated sodium and potassium currents, and an inward rectifier current I_h. These changes result in an action potential that is larger in amplitude and shorter in duration with a more negative voltage threshold. In addition, neurons develop the ability to fire repetitively (Picken Bahrey & Moody 2003).

Such changes in intrinsic properties and the resulting changes in firing properties are likely to influence behavior at the network level. The peak frequency of SSA at stage P0 coincides with a unique time point in neuronal characteristics. During this period, the expression of voltage-gated sodium channels slowly increases while the membrane resistance slowly decreases to the adult physiological values (Corlew et al. 2004). In addition, the rate of increase of sodium channel expression exceeds that of potassium channel expression and occurs earlier during development (Picken Bahrey & Moody 2003). Thus, at the peak of SSA frequency, the sodium current density is much greater than the potassium current density; by P5, however, the potassium current expression has increased such that the two currents are roughly equal in density. This particular configuration of ion channels allows neurons to adapt their responses to appropriately represent the scale of the incoming stimulus, which they cannot do earlier in

development (Mease et al. 2013). Changes in the intrinsic properties of neurons are expected to contribute to the overall network behavior, and understanding such intrinsic properties in the case of SSA may provide further insight into the mechanisms of wave generation. In the cerebral cortex, we are able to specifically target the population of cells which initiate SSA and compare their properties to cells which do not initiate SSA.

In this work, we investigated the differences in neuronal properties and behavior between the ventral and dorsal region. In chapter 1, I will discuss experiments in which we used calcium imaging to observe the behavior of neurons in the piriform cortex and dorsal neocortex during the developmental period during which SSA reaches its peak frequency. We asked whether asynchronous spontaneous activity generated during time periods between synchronous waves in individual neurons differed between piriform pacemaker and dorsal follower regions, and whether such differences were due to synaptic circuitry or cell-autonomous firing properties. We found that individual neurons in the piriform cortex generated a higher level of asynchronous activity than neurons in dorsal neocortex and that this activity remained in the presence of synaptic antagonists, suggesting that it results from intrinsic cellular properties that differ between the two regions. In addition, we observed clusters of ten to two hundred cells synchronously activated in the absence of global SSA. These clusters were more densely distributed in the piriform cortex compared to the neocortex and were reduced by the application of octanol, an antagonist of gap junctions. In addition, I will describe findings from electrophysiological recordings of neurons in the ventral and dorsal regions. In these recordings, we observed a difference in both the frequency of giant depolarizing potentials (GDPs) thought to correlate with the calcium events observed in imaging studies and the frequency of excitatory

postsynaptic potentials (EPSPs) supporting the theory that there is a higher level of intrinsic activity in the ventral region.

In chapter 2, I will describe the development of a computational model designed to test the general hypotheses derived from our experimental findings and the results of the model simulations. To investigate the interactions between activity patterns in the different cortical regions and the postulated contributions of gap junctional connectivity, we constructed a conductance-based network model consisting of three layers of neurons. To simulate our experimental findings, we gave a subset of the model neurons the ability to spontaneously and autonomously generate bursts of action potentials. The proportion of the such neurons was varied among layers. This model was able to generate propagating waves of SSA initiated in the ventral region, using the ventrally-weighted occurrence of spontaneous asynchronous activity as the only spatial asymmetry in the model.

CHAPTER 1

Spontaneous synchronous activity (SSA) in the neonatal mouse cortex provides a unique experimental opportunity to investigate the mechanisms of generation of synchrony due to the ability to directly compare a region that initiates SSA, the ventral piriform cortex, with a region that does not, the dorsal neocortex. This particular situation provides a comparison between two conditions determined by the physiology of the biological system rather than by experimental manipulation. Thus, the goal in these studies was to investigate the differences between the neurons in the ventral and dorsal cortex to understand the properties in the ventral cortex that permit SSA generation.

In order to characterize the properties in these two cortical regions, we used calcium imaging and whole-cell patch clamp electrophysiology. We investigated the activity of single neurons and small groups of neurons in the period between global synchronous events. We found that the ventral cortex had a higher proportion of asynchronously active cells and a greater frequency of synchronous groups of cells than the dorsal cortex. When we applied a combination of synaptic antagonists, asynchronous activity in single cells and groups of cells remained intact, indicating that asynchronous activity is produced by cell-autonomous mechanisms that do not rely on synaptic transmission. In addition, we found that asynchronous activity required voltage-gated calcium channels, and small-scale synchrony required gap junctions.

These results indicate a substantial difference in the level of physiological activity intrinsic to the ventral and dorsal cortex. We hypothesized that this difference could explain the ability of the ventral cortex to generate SSA in contrast to the dorsal cortex. In order to test this hypothesis, we built and tested a computational model simulating our experimental findings. These modeling studies are described in Chapter 2.

Methods

Tissue Preparation and Culture

All procedures were performed in accordance with the guidelines of the NIH and were approved by the University of Washington IACUC. Swiss-Webster mice purchased from Harlan (Indianapolis, IN) and CD1 mice provided by R. Hevner (Seattle Children's Research Institute Center for Integrative Brain Research) were time-mated, and pregnant females were euthanized on embryonic day E17 by CO_2 narcosis followed by cervical dislocation. No differences were found between data obtained from the two mouse strains; therefore, all data was pooled for analysis. Fetuses were removed, decapitated, and the brains dissected in ice-cold artificial cerebral spinal fluid (ACSF; see Solutions and Drugs) equilibrated with carbogen gas (95% O_2– 5% CO_2). The brains were sectioned into 300 μm thick coronal slices in ice-cold ACSF using a Leica VT1200S vibrating microtome. Slices were cultured in an H_2O-jacketed incubator at 36-37ºC in 5% CO_2 on sterilized Millicell culture plate inserts (Millipore Corporation, Billerica, MA) in 1 mL cell culture medium (see Solutions and Drugs). Culture media was changed every other day. Experiments were performed on slices from E18 to P2 (E17 + 1-4 days in culture).

We used cultured coronal slices because this was the preparation we used in previous experiments to demonstrate that spontaneous waves were driven by a pacemaker in the piriform cortex, and our goal in this study was to ask whether intrinsic asynchronous spontaneous activity in neurons of that pacemaker region differed from that in dorsal, non-pacemaker regions. We have recorded spontaneous waves in both horizontal (Corlew et al., 2004) and sagittal slices (unpublished). We used cultured slices also to avoid problems caused by damaged surface-layer cells, which can, for example, show altered chloride gradients and GABA function (Dzhala et al., 2012). In our experience, surface cells in cultured slices are much healthier than in acute slices,

as judged both by appearance and by whole-cell recordings (see e.g., McCabe et al., 2007). We have shown previously that many parameters of electrophysiological development (capacitance, voltage-gated sodium and potassium currents, spontaneous waves of activity; McCabe et al., 2006) as well as migration of interneurons (unpublished) occur similarly in acute and cultured slices.

Solutions and Drugs

Cell culture medium was comprised of 75% sterile Neurobasal-ATM Medium (13) (Invitrogen, Carlsbad, CA), 25% horse serum (Sigma), penicillin (100 IU/mL), streptomycin (0.1 mg/mL), and 2 mM L-glutamine (HyClone Laboratories, Logan, UT). Artificial cerebrospinal fluid contained 140 mM NaCl, 3 mM KCl, 2 mM $MgCl_2$, 2 mM $CaCl_2$, 1.25 mM $NaHPO_4$, 26.5 mM $NaHCO_3$, and 20mM D-glucose in millipore water. The cocktail of synaptic antagonists contained 10μM picrotoxin, 10μm D-AP5, and 25μm CNQX in ACSF. Tetrodoxin and $CdCl_2$ were prepared at concentrations of 1 μM and 100 μM, respectively. Drugs were obtained from Tocris Bioscience (Ellisville MO, USA), and salts were obtained from Sigma (St. Louis, MO).

Ca2+ Imaging

Slices were removed from the incubator and allowed to rest for 1 hour in warmed, oxygenated ACSF and then immersed in oxygenated ACSF containing 1.5 μm fluo-4AM, a calcium indicator dye, and 0.07% Pluronic Acid (Molecular Probes, Eugene, OR) for 40 minutes. Slices were then placed in the recording chamber and allowed to rest for 30 minutes. High-resolution videos were obtained with an Olympus BX51WI microscope using a 20x water immersion objective. Images were captured with a CoolSnap ES camera (Photometrics, Tucson, AZ) using an exposure time of 300 ms with an interval of 1.0 s. Wide-field imaging was done with a Nikon AZ100 microscope with a 2x objective and a Photometrics QuantEM 512SC or an

Orca Flash 2.8 camera. All data collection was done with NIS Elements software (Nikon Instruments, Melville, NY). During imaging slices were continuously perfused with oxygenated ACSF at 30-32 ºC. After control traces were obtained, drugs were washed in for 30 minutes (45 minutes for $CdCl_2$) before reimaging under the treatment condition.

Electrophysiology

Electrophysiology experiments were conducted in Swiss–Webster neurons from coronal cortical slices cut at E17 and cultured for 2-5 days. Patch pipettes were pulled to a resistance of 8-12 MΩ from 50 µl hematocrit glass capillary tubes using a two-stage puller (Narishige), and filled with potassium internal solution, which contained the following (in mM): 105 potassium gluconate, 28 KCl, 2 MgATP, 3 Na2ATP, 0.2 NaGTP, 10 HEPEs, 1 EGTA, pH to 7.25. During recording, tissue was maintained in ACSF at 30-32°C bubbled with carbogen gas (95% O_2-5% CO_2). All salts were obtained from Sigma. Recordings were made using a List EPC-7 (Heka Elektronik) amplifier. The number of excitatory postsynaptic potentials were counted by hand in 6 ventral cells (4 slices) and 6 dorsal cells (5 slices).

Data Analysis

High resolution imaging. Data were exported from NIS Elements as a series of tiff images and analyzed in Matlab. Individual neuron borders were detected using Caltracer 2 (available through: http://www.columbia.edu/cu/biology/faculty/yuste/methods.html) with the standard parameters. Raw fluorescence traces from individual neurons were exported for further analysis. Background regions were selected where cells were not present in the image, and their scaled fluorescence average was subtracted from identified cells to correct for baseline fluctuations in illumination. After baseline subtraction, fluorescence traces were detrended to account for photobleaching over the course of the experiment. Detrending was accomplished

using the preprogrammed Matlab detrend function which removes linear trends using fast Fourier transform analysis. Calcium transients in individual cells were detected based on an analysis of the time derivative of the change in fluorescence vs. mean fluorescence ($\Delta F/F_0$), where ΔF represents the change in the fluorescence intensity between subsequent frames and F_0 represents the mean fluorescence of an individual cell over the course of the imaging trial. Positive deviations of $d(\Delta F/F_0)/dt$ greater than two standard deviations were identified as the start of calcium transients. For a neuron to be included for analysis, it was required that the $\Delta F/F_0$ signal to reach a threshold between 0.02 to 0.1 which was set independently for each slice, based on the level of noise and intensity of the fluorescence signal present in the images. The largest value of $\Delta F/F_0$ in a calcium transient was identified, and all of the smaller transients had to reach a proportion (0.2 - 0.4) of this value to be counted. This threshold proportion was set independently for each slice based on the fluorescence decay and the level of noise to prevent inclusion of small noise fluctuations as events. Additionally, neurons with noise levels indistinguishable from calcium transients were excluded from analysis. After detection of events in all identified cells in the field of view, the average number of cells active during each frame (1.3 seconds) was determined, and the occurrence of global synchrony was defined as those time points during which the number of cells active in a single frame exceeded the mean plus twice the standard deviation. If the mean plus twice the standard deviation of the activity per frame was less than five, we used five as an alternative minimum; this was necessary for imaging trials in which particular drug treatments (e.g., $CdCl_2$) resulted in very low levels of cellular activity.

Wide-field imaging. Images in the form of tiff stacks were imported into MatLab, corrected for bleaching, and converted into $\Delta F/F_0$ images. Activity was thresholded at twice the standard deviation of baseline F noise and then superimposed back onto a camera image of the

slice. Superposition was done destructively, by zeroing all camera image pixels underneath the supra-threshold activity to maintain accuracy of the $\Delta F/F_0$ numbers. To detect the spatial distribution of asynchronous activity of cells and clusters, thresholded activity was accumulated for a given stack, and the summed activity superimposed onto a camera image of the slice (see Fig. 1A, e.g.). Cells and clusters were separated by total pixel area (2-20 pixels for cells, and >20 pixels for clusters for a 512 x 512 image). Temporal plots of the activity of individual cells and clusters was done in MatLab by detecting active objects, using the pixel lists of those objects to create masks, and then plotting mean pixel intensity *vs.* time within each mask over the time course of the image stack.

Statistical analyses. Statistical significance was calculated using the Student's t-test. A paired test was used to compare control and experimental conditions when a single slice was exposed to a pharmacological treatment and in the analysis of wide-field imaging data for comparisons between the dorsal and ventral when imaging of both regions was simultaneous. An unpaired heteroscedastic test was used for unpaired data comparing ventral and dorsal data that was obtained sequentially or from different slices. All data are presented as mean ± S.E.M. The number of samples, *n*, for each experiment is the number of slices, unless otherwise indicated. Slices were not used for more than one experiment (a single unpaired trial or a control and an experimental trial) due to bleaching of the calcium indicator dye.

Results

Films of spontaneous calcium transients occurring between spontaneous synchronous waves of activity in coronal slices (E18 – P2; E17 + 1-4 DIV) revealed two types of spontaneous activity. As shown in Supplemental Movie 1, individual neurons showed spontaneous calcium transients, and small clusters of neurons were also synchronously active. Figure 1A shows a summation of all frames in this 10 minute recording, so that each cell that was active at least once is marked. During this time, 8 clusters (an example is marked by the white arrow) and more than 50 individual cells (red arrow) were active.

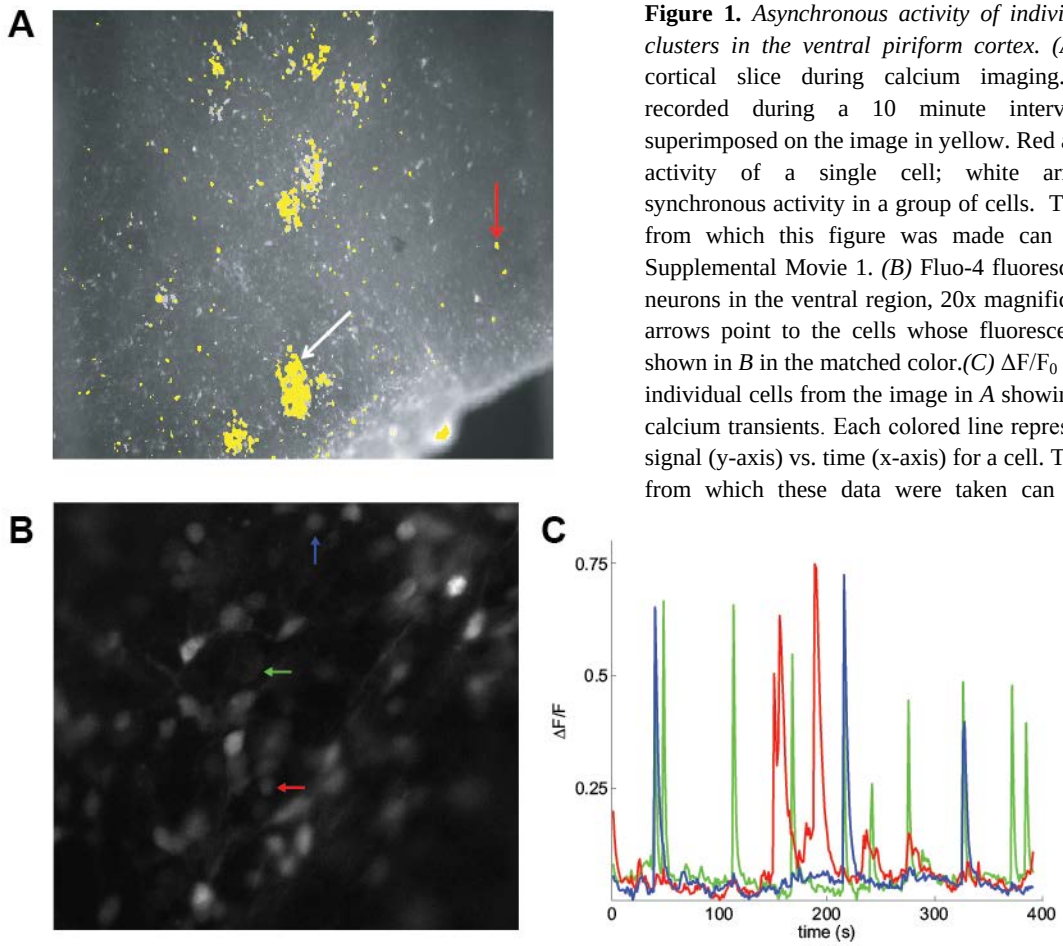

Figure 1. *Asynchronous activity of individual cells and clusters in the ventral piriform cortex. (A)* Image of a cortical slice during calcium imaging. All activity recorded during a 10 minute interval is shown superimposed on the image in yellow. Red arrow indicates activity of a single cell; white arrow indicates synchronous activity in a group of cells. The image stack from which this figure was made can be viewed as Supplemental Movie 1. *(B)* Fluo-4 fluorescence image of neurons in the ventral region, 20x magnification. Colored arrows point to the cells whose fluorescence traces are shown in *B* in the matched color.*(C)* $\Delta F/F_0$ traces for three individual cells from the image in *A* showing spontaneous calcium transients. Each colored line represents the $\Delta F/F_0$ signal (y-axis) vs. time (x-axis) for a cell. The image stack from which these data were taken can be viewed as

Asynchronous activity in individual cells between waves of synchronous global activity

Individual neurons showed spontaneous calcium transients in the period between waves of activity. Figure 1B shows a fluorescence image of a field of cells in the ventral piriform cortex, along with a plot of $\Delta F/F_0$ signals from three of these cells. A film of this field of view is shown in Supplemental Movie 2. On average, 37 ± 2.8 % of detected cells in the piriform cortex showed at least one spontaneous calcium transient within a 390 second imaging period (*n* = 19). Within that subset of cells that showed spontaneous activity, the average frequency was 0.543 $\pm$ 0.010 events/min (19 slices, 1951 cells).

In order to determine if asynchronous activity differs regionally, we used calcium imaging with single-cell resolution in 19 ventral and 12 dorsal regions in cultured cortical slices between P0 and P2. We found that in both the ventral and the dorsal cortex, some neurons were active between spontaneous waves. The number of neurons displaying asynchronous activity in the ventral cortex was significantly greater than in the dorsal cortex. Figure 2A displays the number of active cells in 1 second time bins during a typical recording in dorsal neocortex and ventral piriform cortex (*right*) and an image of the summation of all cells asynchronously active during a 3 min interval (*left*). Figure 2B quantifies the proportion of active cells relative to all cells detected for all recordings in dorsal and ventral cortex, and shows that the ventral regions contained a larger proportion of active cells than dorsal regions. In 19 ventral experiments, 37 ± 2.8 % of cells were asynchronously active compared to 9.6 ± 1.4 % in 12 dorsal experiments ($p < 10^{-8}$). Table 1 lists the properties of synchronous and asynchronous events measured in the dorsal and ventral cortex in these experiments.

Table I. Asynchronous and synchronous event properties.

	Ventral	Dorsal	p-value
Synchronous event frequency	1.3 ± 0.14 min^{-1}	0.23 ± 0.12 min^{-1}	$< 10^{-5}$
Synchronous event fractional participation	0.35 ± 0.16	0.58 ± 0.064	0.002
Asynchronous event frequency (per active cell)	0.54 ± 0.01 min^{-1}	0.56 ± 0.024 min^{-1}	0.4
Calcium transient amplitude ($\Delta F/F_0$)	0.299 ± 0.0039 ($\sigma = 0.4690$)	0.138 ± 0.0035 ($\sigma = 0.1526$)	< 0.001

Data collected from: 19 ventral slices (157 synchronous events, 1951 cells showing asynchronous activity, and 14478 calcium transients) and 12 dorsal slices (18 synchronous events, 316 cells with asynchronous activity) and 1914 calcium transients. Values represent mean ± s.e.m.

To ensure that these differences were not due to the time of recording or other factors present when dorsal and ventral recordings were done sequentially, we used low-power wide-field imaging (see Methods) to detect spontaneously active cells simultaneously in dorsal and ventral regions of 28 slices between E18 and P2 (E17 + 1-4 DIV). To ensure that our thresholding to separate synchronous and asynchronous activity in the high-power narrow-field imaging above accurately detected spontaneous waves, we compared wave frequencies measured in those experiments to those measured directly by detection of propagating waves in whole-slice experiments. Both ventral and dorsal wave frequencies were the same in both experiment types: ventral (1.27 ± 0.14, narrow-field, *vs*. 1.70 ± 0.62, wide-field, $p=0.54$); dorsal (0.23 ± 0.12, narrow-field, *vs*. 0.23 ± 0.10, wide-field, $p=1.0$; $n = 340$ events in 28 slices). As expected from the fact that fewer than 20% of waves propagate out of the piriform cortex into the neocortex at these stages (Conhaim et al., 2011), the frequency of synchronous events detected dorsally is much lower than ventrally.

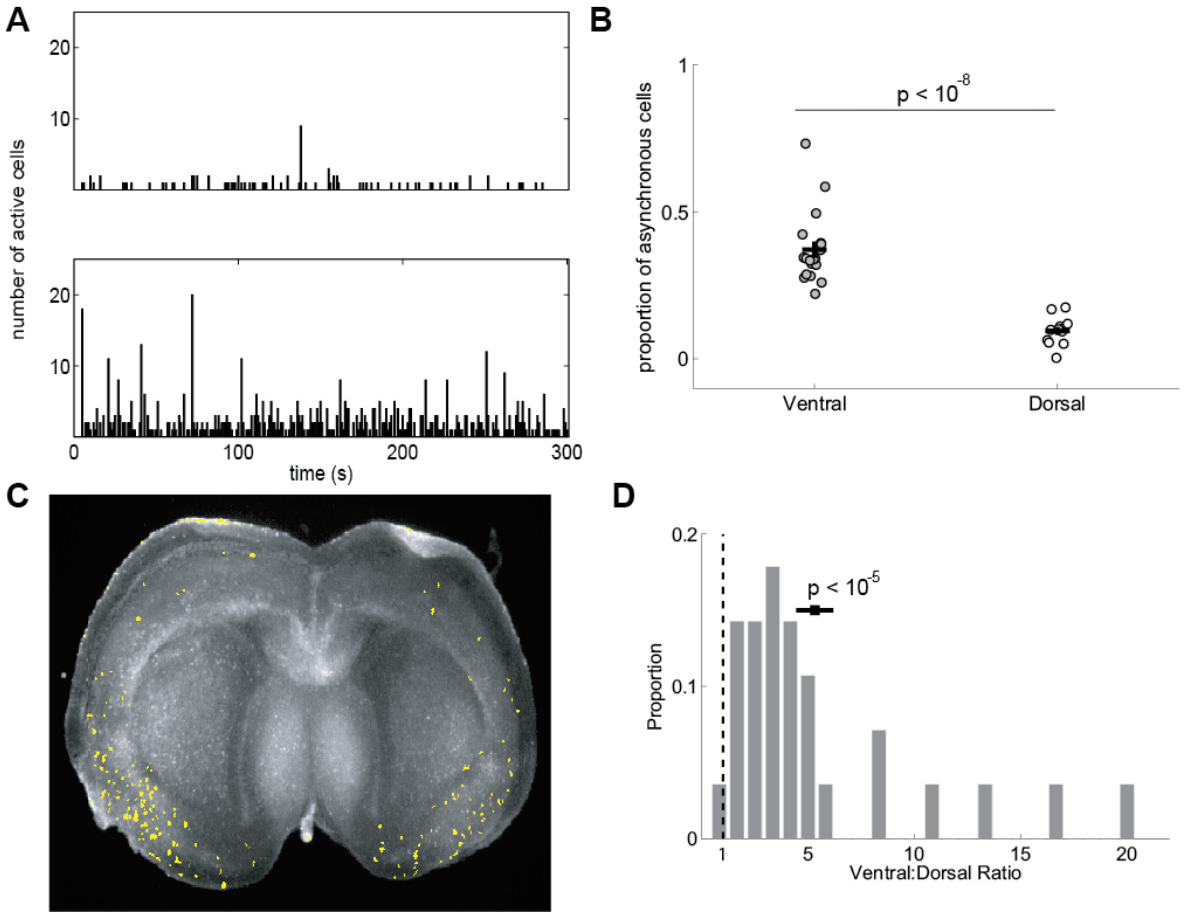

Figure 2. *Comparison of single-cell asynchronous activity in the ventral and dorsal cortex.* (A) Examples of single-cell activity in dorsal (top) and ventral (bottom) regions. Black bars represent the number of cells active in each 1 sec time bin. Synchronous events (see Methods) were removed and the number of cells at those time points set to zero. (B) Proportion of cells with asynchronous activity in ventral (*left, n = 19)* and dorsal (*right, n = 12*) regions in the 390 s imaging period. Each circles represents one experiment. Black crosses represent the mean, with the height of the vertical bar showing the s.e.m. (C) Image of a coronal slice with all cells showing $\geq$ spontaneous Ca transients during the 3-min recording period marked in yellow. Note that the number of active cells is higher in the ventral (piriform) cortex bilaterally. (D) Histogram of the ratio of ventral:dorsal active cells in 28 whole-slice imaging experiments such as that shown in C. Black cross marks the mean and the vertical bar the s.e.m. The dashed line shows a ratio of 1.0.

Figure 2C shows a slice image with each cell that showed at least one spontaneous calcium transient during the 3-min recording period marked. The ventral cortex bilaterally had substantially more active cells than dorsal cortex. This difference as detected in wide-field imaging experiments is quantified in Figure 2D, a histogram of the ratio of the number of asynchronously active ventral cells to the number of asynchronously active dorsal cells per unit area in each experiment. This quantification shows that the number of cells with spontaneous

activity between synchronous waves in ventral cortex was 3 times higher (36.9 $\pm$ 5.6 cells/min/mm^2) than in dorsal cortex (12.0 $\pm$ 2.0 cells/min/mm^2; $p<10^{-5}$). The mean frequency of asynchronous activity did not differ between the ventral (0.543 ± 0.010 events/min, 1951 cells) and dorsal (0.564 ± 0.024 events/min, 316 cells) cortex (p = 0.43; high resolution imaging).

Together these data show that in the pacemaker region of the piriform cortex, which initiates more than 99% of all spontaneous waves (Lischalk et al. 2009), a larger fraction of cells show spontaneous calcium transients between waves than in the non-pacemaker dorsal cortex.

Synaptic isolation via synaptic antagonists does not eliminate asynchronous activity in individual neurons.

During the E18 – P2 period, neurons rely on developing GABAergic and glutamatergic synapses for chemical transmission. In order to determine if the differences in single cell asynchronous activity between ventral pacemaker and dorsal follower regions reflects differences in synaptic circuitry or in intrinsic cellular properties, we perfused 9 ventral and 10 dorsal cortical slices between E18 and P2 with a combination of CNQX, an AMPA receptor blocker, AP5, an NMDA receptor blocker, and picrotoxin, a $GABA_A$ receptor blocker and observed the effects on activity. In agreement with previous data (Conhaim et al. 2011), synaptic isolation eliminated synchronous global activity in both ventral and dorsal regions (Fig. 3A,B,D; p = 0.001 ventral, p = 0.04 dorsal). Note that this figure also shows that the frequency of synchronous events is lower in the dorsal than in the ventral cortex, as expected from the fraction of waves that propagate into the dorsal cortex from the piriform pacemaker at these stages (Conhaim et al., 2011). This further confirms that the synchronous events we detect at the

single-cell level correspond to the propagating waves seen in whole-slice imaging. Despite the elimination of synchronous activity, a significant proportion of cells in both ventral and dorsal cortex remained asynchronously active in the presence of the combination of synaptic blockers (Fig. 3A,B,C). In the ventral cortex, synaptic isolation reduced the percentage of asynchronously active cells from 33 ± 2.8 to 25 ± 3.9 % (n = 9; p = 0.01). In the dorsal cortex, the reduction was from 9.0 ± 1.6 to 6.0 ± 0.86 % (n = 10; p = 0.04). In both cases, however, the proportion of asynchronously active cells was significantly greater than zero ($p < 10^{-5}$, ventral; $p < 10^{-3}$, dorsal) and the ventral/dorsal ratio of asynchronously active cells was similar under synaptic isolation (4.2) and under control conditions (3.7), (p = 0.001, ventral vs. dorsal proportions of asynchronous cells under synaptic isolation). These results indicate that developing neurons have a cell-autonomous mechanism for producing calcium transients in the absence of synaptic input, and that although a fraction of asynchronous activity depends on synaptic inputs, the higher proportion of spontaneous active cells ventrally primarily reflects a difference in intrinsic cellular properties between these two regions.

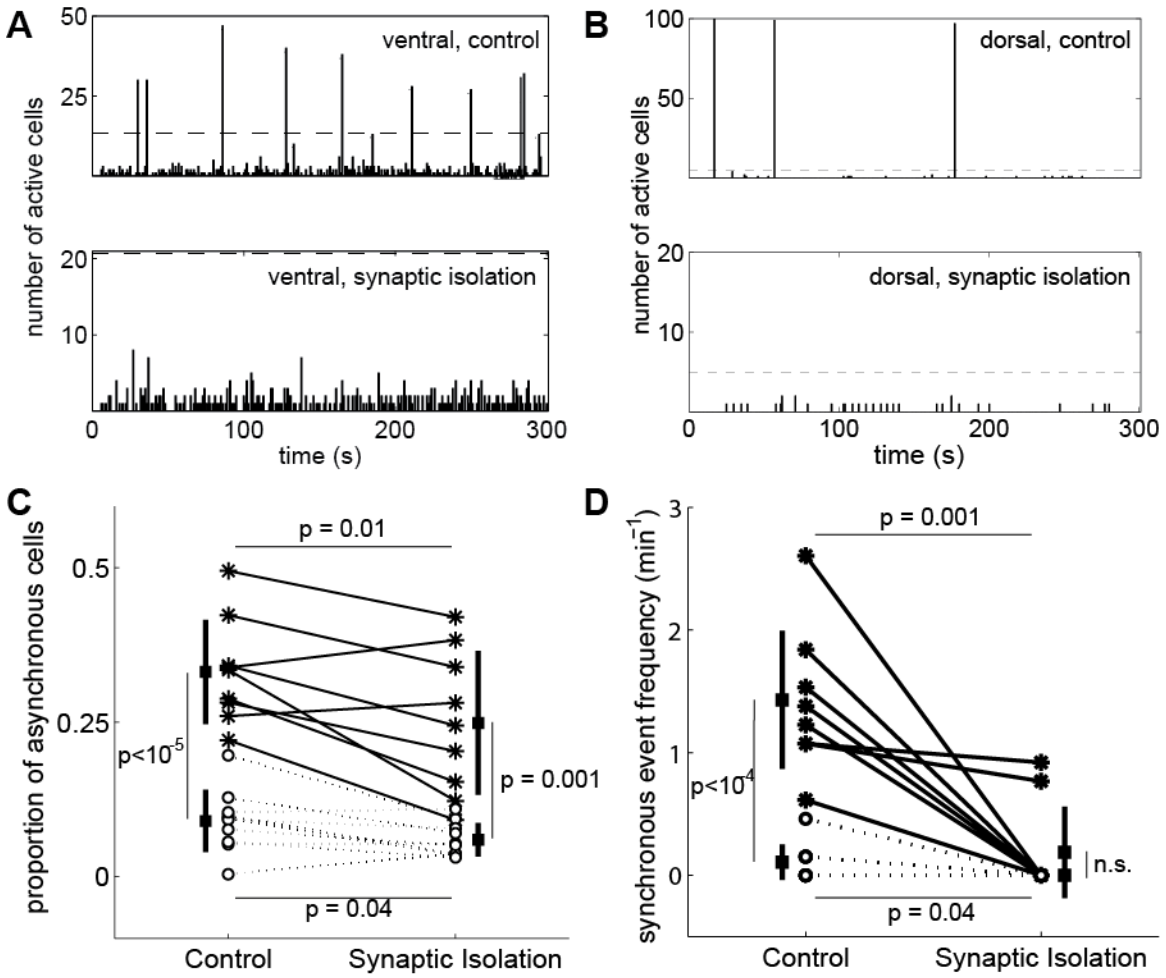

Figure 3. *Effects of synaptic isolation on synchronous and asynchronous activity in the ventral and dorsal cortex. (A)* Example of activity in ventral region before *(top)* and after *(bottom)* synaptic isolation. Black bars represent the number of cells active at each time point. Synaptic isolation blocks synchronous events but leaves asynchronous activity intact. *(B)* Same as in *A* for dorsal region. Note that for both plots, the vertical scale is different for control and drug data. *(C)* Proportion of cells asynchronously active before *(left)* and after *(right)* synaptic isolation in paired experiments. Ventral experiments are shown with grey circles and solid black lines *(n = 9)*. Dorsal experiments are shown with white circles and dashed lines *(n = 10)*. Black squares represent the mean. Black bars show the s.e.m. Not significant = n.s.; p-values are given. Asynchronous activity in both ventral and dorsal regions is not blocked by synaptic isolation. *(D)* Frequency (min^{-1}) of synchronous events before *(left)* and after *(right)* synaptic isolation in paired experiments, confirming block of synchronous waves by synaptic isolation.

Spontaneous activity in clusters of cells between synchronous waves

As shown in Figure 1A (and Supplemental Movie 1), coactive clusters of cells were seen between synchronous waves as well as the individual active cells described above. In the experiment shown in Figure 1A, 8 such clusters were detected during the 10 minute imaging time. Single clusters rarely were active more than once during a single experiment, but the

overall occurrence of clusters in the ventral cortex was 4.46 ± 0.54 clusters/min/mm^2 (n = 29), about nine times lower than the average activity of individual cells measured in the same way (36.9 ± 5.6 cells/min/mm^2).

Figure 4 shows activation of a typical cluster. Activity starts with a single centrally-located cell and spreads radially outward over the course of 3-10 seconds to encompass a roughly spherical group of cells. We calculated the number of cells per cluster by extrapolating cell counts in a single plane of focus to an assumed spherical geometry, which gave a mean value of 77.0 ± 9.7 cells/cluster (n=77 clusters). The distribution of cluster sizes was not symmetrical (Fig. 5), showing a median of 43 cells and a small number of very large clusters which were difficult to distinguish from local synchronous waves.

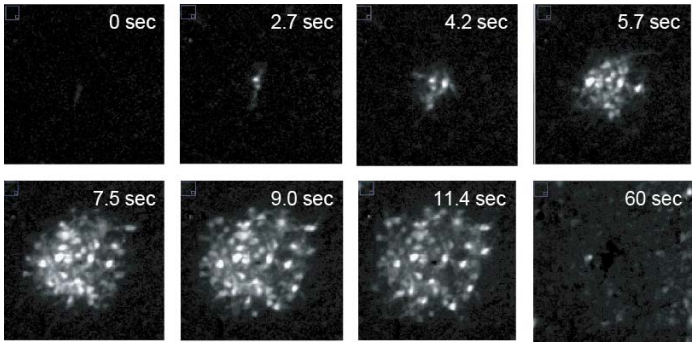

Figure 4. *Activation of a cellular cluster.* Individual frames from a calcium imaging experiment. Times are given in the upper right corner of each image. Cluster activation starts with a single active cell and then spreads radially over the course of 10-11 sec.

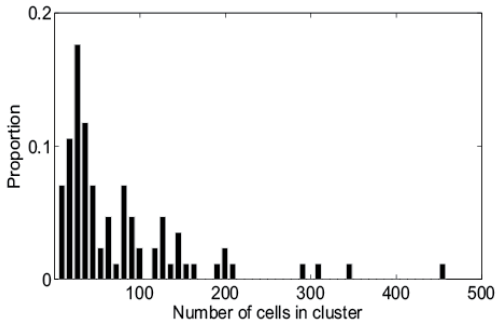

Figure 5. *Distribution of cluster size.* Histogram of the number of cells in each detected cluster. Total number of clusters was 77. Average number of cells/cluster was 43.

Most clusters were initiated by activity in a single central cell, as shown in Figure 4. Other clusters, however, appeared to be triggered by a central cell whose baseline fluorescence level was high, and decreased abruptly as surrounding cells of the cluster became active. An example of this kind of "off cell" cluster is shown in Figure 6. In a sample of 56 clusters in which we could distinguish either center "on" or "off" cells clearly, 24 (43%) showed central

"off" cells. This is likely to be an underestimate because if initial activation of clusters is rapid compared to image capture frequency, it is easier to detect a cell whose calcium signal decreases and stays low than a cell whose signal increases before surrounding cells.

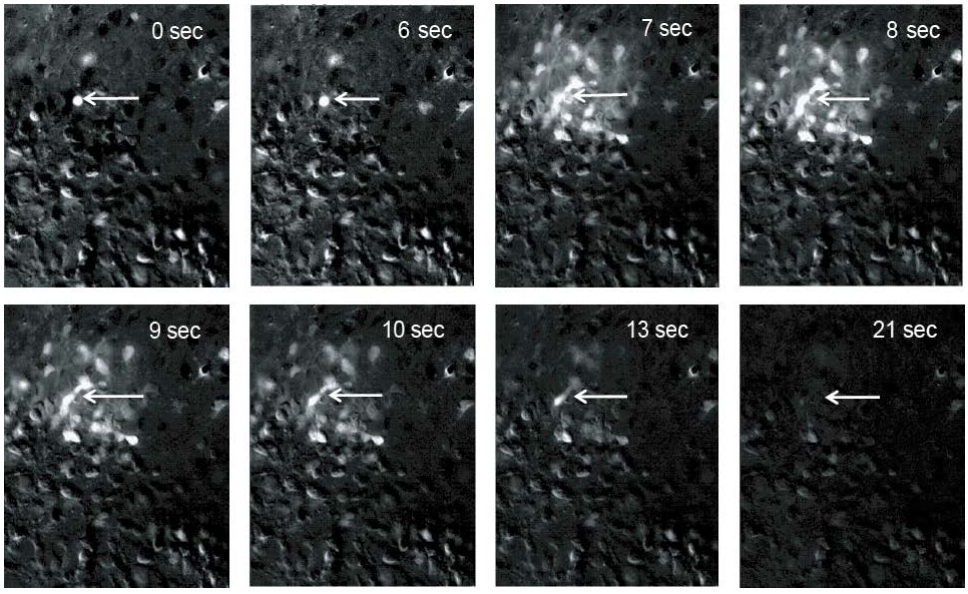

Figure 6. *Activation of a cellular cluster triggered by an 'off' cell.* Individual frames from a calcium imaging experiment. Times are given in the upper right corner of each image. The central cell is indicated by a white arrow. The decrease in fluorescence of the central cell is seen in the third panel simultaneous with the activation of the cluster.

The patterns of activity in clusters did not appear to correspond to the presence of discrete groups of connected neurons. Individual cells often participated in the activity of more than one cluster. Figure 7A shows an example of sequential activity in two spatially contiguous clusters, with several cells at the border between the two clusters participating in both. Figure 7B shows another example of three nearby clusters active with no overlap in participating cells in two of the clusters, but approximately 50% overlap in participating cells in the other two clusters. Further analysis showed that individual cells could participate sequentially in single cell asynchronous activity, cluster activity, and in synchronous waves within a single 10-min imaging period.

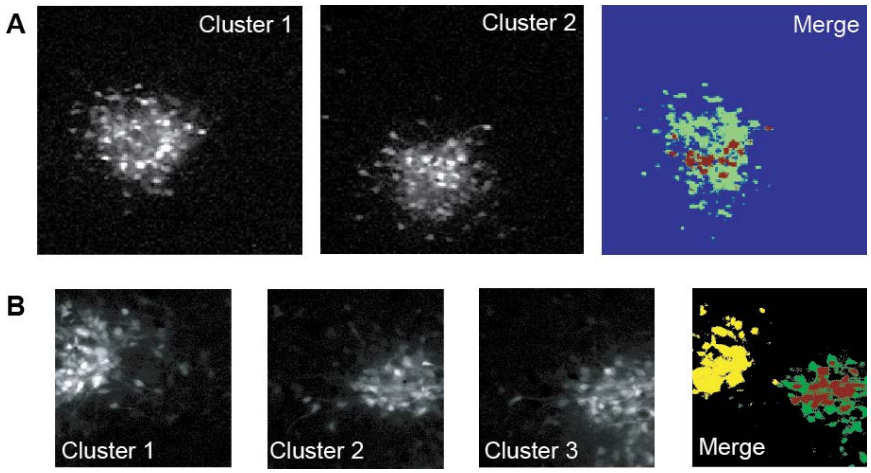

Figure 7. *Overlap of cell participation in clusters. (A)* Two clusters active at different times in the same region are shown in the first two panels. A merge of the two clusters is shown in the third panel. Red indicates cells that participated in both cluster activations. Thresholding to create the merged image results in some cells in each cluster not displayed. *(B)* Three cluster activations are shown in the first three panels. In the merged fourth panel, red indicates cells active in both the second and third clusters. Cell activity from panel 1 is show in yellow and did not overlap with either of the other two clusters.

Active clusters occur more often in the ventral pacemaker region

We next asked whether clusters showed a higher probability of occurrence in the ventral piriform region than in the dorsal cortex, using the same wide-field imaging analysis that showed the preferential ventral distribution of single cell activity (Fig. 2C). Figure 8A shows an image of all active clusters detected in a single coronal slice during a 3-min imaging period. Active clusters are preferentially clustered in the ventral cortex bilaterally. Mean cluster occurrence derived from 29 such slices was 4.46 $\pm$ 0.54 clusters/min/mm^2 in ventral cortex *vs.* 0.49 $\pm$ 0.10 clusters/min/mm^2 in dorsal cortex ($p < 0.001$) (Fig. 8B).

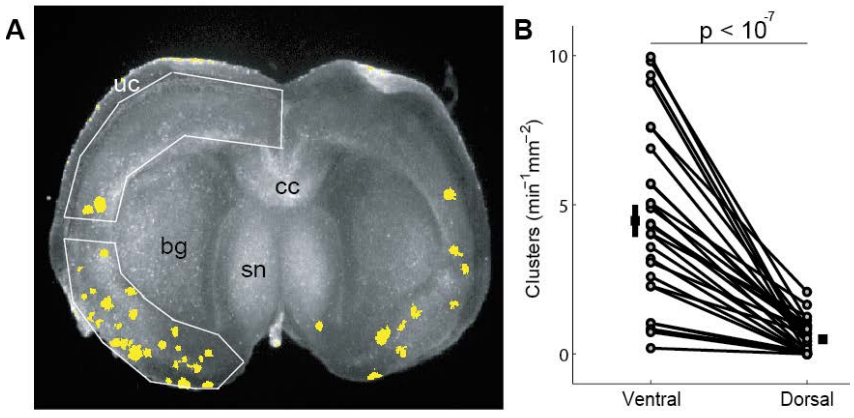

Figure 8. *Spatial distribution of cellular clusters in the ventral and dorsal cortex. (A)* Image of a cortical slice during calcium imaging. All clusters that were active during the 10 minute imaging time are shown superimposed on the image in yellow. White outlines show the division between dorsal and ventral cortex used for quantification. *uc* = uncut edge of slice, not included in quantified regions; *bg* = basal ganglia; *cc* = corpus callosum; *sn* = septal nucleus. *(B)* Frequency (min^{-1}mm^{-2}) of clusters in ventral (*left*) and dorsal (*right*) regions during each experiment. Black squares represent the mean. Black bars show the s.e.m.

Asynchronous activity depends on voltage-gated calcium channels but not on sodium channels.

In order to investigate the mechanism behind the generation of autonomous activity in developing neurons, we perfused cortical slices between P0 and P2 with antagonists of membrane ion channels. We examined the effect of tetrodotoxin (TTX), which blocks voltage-gated sodium channels, on two ventral and two dorsal regions. As seen in previous studies, TTX eliminated synchronous global events (Fig. 9B; $p = 0.02$, $n = 8$), confirming that sodium-spike dependent synaptic transmission is required for spontaneous waves; however, TTX did not eliminate asynchronous activity between waves (Fig. 9A; $p = 0.14$, $n = 4$). In contrast, 100 µM cadmium chloride, which non-specifically blocks voltage-gated calcium channels, eliminated both synchronous (Fig. 9B; $p = 0.02$, $n = 5$) and asynchronous (Fig. 9A; $p = 0.001$, $n = 5$) activity in four ventral slices. Thus, we surmise that the mechanism responsible for generating autonomous activity in the absence of synaptic input is not dependent on sodium channels but is dependent on voltage-gated calcium channels. A voltage-gated calcium channel mechanism is necessary for asynchronous activity, which may or may not be augmented by internal calcium release.

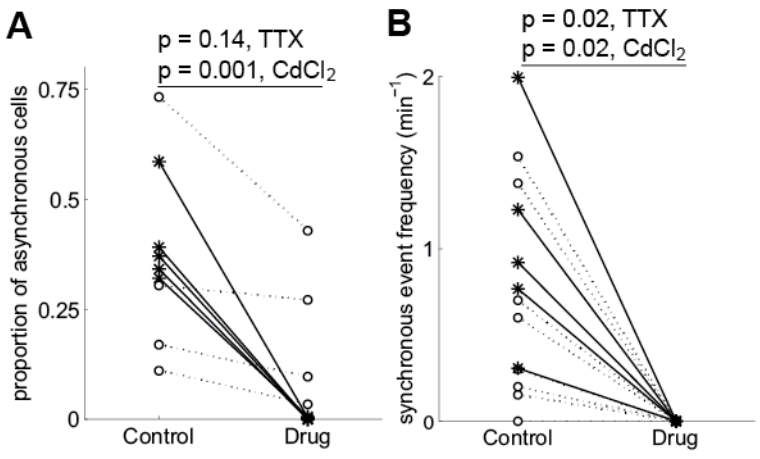

Figure 9. *Effects of voltage-gated ion channel antagonists on synchronous and asynchronous activity*. *(A)* Proportion of cells with asynchronous activity under control conditions (*left*) and application of TTX or $CdCl_2$ *(right*). Grey circles and solid lines represent application of $CdCl_2$ (*n = 5*). White circles and dashed lines represent application of TTX (*n = 4*). Lower two TTX experiments are from dorsal regions. *(B)* Frequency of synchronous wave activity (min^{-1}) under control conditions (*left*) and after application of TTX (*n = 8*) or $CdCl_2$ (*n = 5)*. In both panels, lines connect data from the same imaging runs before and after drug application.

It is of course possible that cadmium blocks the pathway for calcium entry during activity, thus eliminating the signal we measure, without completely blocking the electrical activity. The lack of TTX sensitivity of asynchronous activity makes this interpretation less likely, however, because it argues against the idea that cadmium blocks calcium entry during activity while leaving activity based on voltage-gated sodium channels intact. If electrical activity were based on sodium channels and the calcium signal were based on internal release, we would expect TTX to eliminate the electrical activity and its triggering of an internal release of calcium.

If asynchronous electrical activity in a subset of neurons does in fact underlie the different abilities of neocortex and piriform cortex to act as pacemakers for spontaneous waves, then piriform neurons should show higher frequencies of synaptic activity than neocortical neurons, as a result of their having inputs from a greater proportion of asynchronously active neighbors. To test this, we made whole-cell current clamp recordings from 6 ventral neurons in 4 slices and 6 dorsal cells in 5 slices. In these recordings, ventral neurons showed a significantly higher frequency of EPSPs than dorsal neurons (Fig. 10; 0.57 ± 0.14 min^{-1} in the ventral cortex, 0.122 ± 0.023 in the dorsal cortex, $p = 0.006$). These data indicate that increased asynchronous activity in the ventral cortex is reflected in increased synaptic drive onto those cells which, in turn, is likely to increase the probability of periodic synchronization of their activity. The average frequency of EPSPs in the ventral cortex is 4.7 times the frequency in the dorsal cortex, somewhat larger than the factors of 3.8 and 3.0 comparing the proportion of ventral to dorsal asynchronously active cells in high-resolution and wide-field imaging, respectively. This difference may represent differences in the connectivity between the two regions.

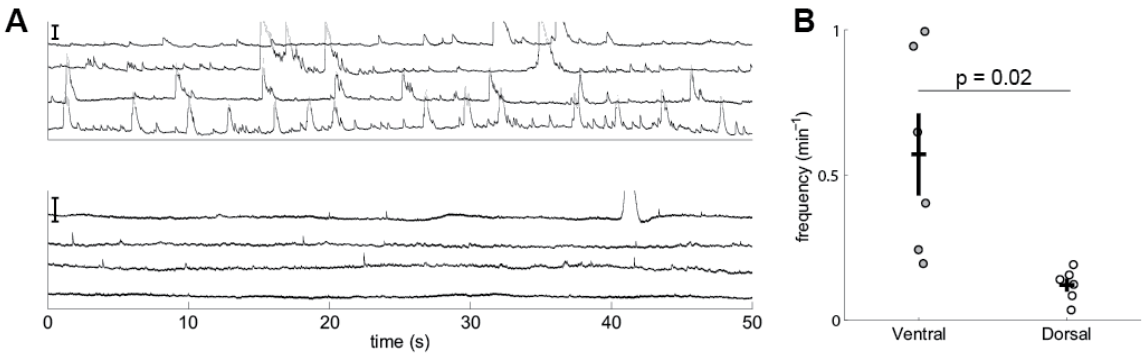

Figure 10. *Frequency of excitatory postsynaptic potentials in the ventral and dorsal cortex. (A)* Sample traces from 4 cells in the ventral(top) and dorsal(bottom) cortex showing the increased frequency of EPSPs in the ventral cortex. Larger calcium events (>20 mV) were excluded form the analysis. Scale bars in the upper left corner of each set of traces represent 10 mV. *(B)* Frequencies (min^{-1}) of EPSPs in the ventral (*n = 6 cells*) and dorsal (*n = 6 cells*) cortex. Black crosses represent the mean. The height of the vertical bar represents the s.e.m.

Clusters are driven by calcium entry and depend on gap junctions

Much like single cell asynchronous activity, clusters persisted in the presence of tetrodotoxin (0.3 $\pm$ 0.09/min, control vs. 0.25 $\pm$ 0.15/min TTX; p=0.8), the combination of CNQX + picrotoxin (1.39 + 0.67/min, control, vs. 0.74 $\pm$ 0.25/min, CNQX+Picrotoxin; p=0.29), and thapsigargin (0.77 $\pm$ 0.21/min, control vs. 1.06 $\pm$ 0.27/min; p=0.46). Like single cell asynchronous activity, cluster activity was completely eliminated by 100µM cadmium (n = 3).

To test the role of gap junctions in the spread of activity within clusters, we applied 3mM octanol. This greatly reduced cluster activity (to 0.048 of control; n = 4 slices; p = 0.029). The fact that single cell activity persisted in the presence of octanol argues against the hypothesis that the action of octanol on electrical activity itself was responsible for the block of cluster activity. Thus, it appears that voltage-gated calcium channels and gap junctions are required for small-scale synchrony in cell clusters.

Discussion

The series of experiments described in this chapter identified key differences between the activity patterns of the ventral and dorsal cortex. Single neurons in the ventral cortex were more likely to demonstrate asynchronous activity during the period between global synchronous waves than neurons in the dorsal cortex. In addition, groups of neurons composing small clusters of synchronous activity were more frequent in the ventral cortex than in the dorsal cortex. In order to determine the origins of this activity, we exposed slices to a combination of synaptic antagonists and found that asynchronous activity persisted. These findings have several implications. First, because synaptic isolation did not eliminate asynchronous activity among cells, asynchronous activity between waves must not be a result of a baseline level of synaptic activity that activates cells when enough inputs arrive simultaneously. Rather, individual neurons must have a cell-intrinsic mechanism that can autonomously produce an influx of calcium. In addition, we found that voltage-gated calcium channels but not voltage-gated sodium channels were necessary for this activity.

Finally, the ability to generate autonomous activity differs between the ventral and dorsal cortex, indicating that neurons in these regions have different intrinsic properties. Neurons in the ventral cortex displayed a greater propensity for autonomous activity. Since this region is responsible for generating SSA, we wondered if the higher level of activity in the ventral cortex could be responsible for the regional differences in large-scale network behavior. If autonomous activity is produced by a sufficient proportion of cells and subsequently amplified by gap junctions, synchronous activity could be triggered in large segments of the neuronal population. Because more of the neurons in the ventral cortex are autonomously active, a synchronous wave would have a greater chance of being triggered compared to the dorsal cortex. It is notable that

we did not observe any instances of reverse propagation of waves from the dorsal to the ventral cortex. This could be due to an insufficient proportion of autonomously active neurons resulting in a generic inability of the dorsal cortex to produce wave or to the higher probability of a ventrally initiated wave which then produces refractoriness in the dorsal cortex. These questions are aimed at an understanding of the fundamental properties that govern the interaction between cell-intrinsic properties, such as the ability to generate autonomous activity, and the behavior of a network. In order to answer these questions, we developed a computational model in which we could manipulate the features of individuals cells and the network architecture. The design and result of this model are detailed in the next chapter.

CHAPTER 2

In order to investigate the interaction between cell-intrinsic properties and network behavior, we built a conductance-based network model to test the hypotheses we formed based on our experimental results. We asked if intrinsic excitability that produces autonomous bursts of spikes in a proportion of neurons within the network could produce synchronous waves of activity without extrinsic input that propagate in one direction. Our experiments showed a low level of synaptic noise occurring in the period between waves; therefore, synaptic noise was an unlikely mechanism by which synchrony could be generated. Imaging experiments that synaptically isolated cells using a combination of synaptic antagonists demonstrated that communication via chemical synapses is not necessary for the generation of uncorrelated activity in single neurons. Therefore, we concluded that neurons must have an intrinsic mechanism by which calcium influx and electrical activity can be triggered. The first aim of the computation experiments was to verify that such a mechanism could generate synchronous waves of activity.

In addition, we aimed to determine if the regionally differing proportions of autonomously active neurons would affect the features of wave propagation. In our experiments, we found that a greater proportion of neurons in the ventral cortex were autonomously active compared to the dorsal cortex, and waves propagate from the ventral to the dorsal cortex. In order to determine if the different distribution of autonomously active neurons is responsible for the directionality of wave propagation, we structured the network with three separate layers of neurons and gave each layer a different proportion of intrinsically bursting neurons such that the proportion changed over space in the same way as our experimental data.

We implemented both synaptic and gap junctional connectivity based on the experimental findings. When synaptic antagonists were applied to cortical slices between E18 and P2, large-scale synchronous activity was eliminated, indicating that the propagation of waves across the cortex relies on synaptic transmission. In contrast, synaptic antagonists did not eliminate small clusters of coactive cells. Local synchrony therefore does not depend on communication via chemical synapses. The activity of these small clusters instead appeared to rely on gap junctions. When octanol was applied to cortical slices, the number of active clusters was dramatically reduced.

This model successfully simulated our experimental findings. By implementing cell-intrinsic bursting in proportions of neurons mirroring those found empirically, we were able to reliably generate waves of activity that propagated from the ventral to the dorsal layer. These findings support our theory that a gradient of autonomously active neurons is sufficient to induce directionally propagating waves .

Methods

Single cell dynamics

The cell-autonomous property of single neurons was based on intrinsically bursting model neurons used by Baltz et al. 2011. These neurons can fire bursts of action potentials without any external input. We used this model for two reasons. First, Baltz et al. 2011 have shown that these neurons best capture initiation of spontaneous activity patterns as observed in cultured developing networks, which correspond to the same developmental periods studied in our slices. Second, simultaneous calcium imaging and patch-clamp experiments in developing cortex have shown that calcium transients are generated by barrages of activity in the network, corresponding to bursts of action potentials riding on top of a long-lasting depolarization recorded in single cells (Alléne et al. 2006).

The model neurons consisted of a single compartment (Smith et al. 2000; Baltz et al. 2011):

$$C_m \frac{dV_m}{dt} = g_L(E_L - V_m) + g_{sra}(E_K - V_m) + I_T + I_{syn}$$

where C_m=1 μF/cm^2 is the specific membrane capacitance, g_L=50 μS/cm^2 is the leak conductance, E_L=-70 mV is the reversal potential of the leak current, and I_{syn} is the synaptic current (see below).The model also includes a transient calcium current I_T

$$I_T = g_T m_\infty h(V - V_T)$$

where V_T=120 mV and g_T=40 μS/cm2. The variable h represents the inactivation of the low-threshold conductance. It relaxes to zero with a time constant τ_{h^-}=90 ms and relaxes back to unity with τ_{h^+}=150 ms:

$$\frac{dh}{dt} = \begin{cases} -h/\tau_{h^-}, & \text{if } V_m > V_h \\ (1-h)/\tau_{h^+}, & \text{if } V_m < V_h \end{cases}$$

This means that when V_m is below V_h= -70.5 mV, the current I_T is deinactivated, and when V_m is above V_h, I_T is inactivated. The activation function is denoted by $m_\infty = \Theta(V_m - V_h)$, where Θ is the Heaviside function. Finally, a negative feedback conductance g_{sra} was added to enable spontaneous bursting (i.e. weak spike rate adaptation), with potassium reversal potential E_K= -75 mV. The frequency of spontaneous bursts mainly depends on the time constant τ_{sra}. We chose this number so that the frequency of spontaneous events was similar to that observed experimentally. In fact, to introduce heterogeneity, τ_{sra} for each neuron was drawn from a Gaussian distribution with mean 8 seconds and standard deviation of 800 ms.

After reaching threshold, V_{th}= -50 mV, the membrane potential was reset to -60 mV and g_{sra} was increased by an amount Δg_{sra}=15 μS/cm2. In addition, a small amount of uniformly distribution random noise was added for slight membrane fluctuations of approximately 0.5 mV that did not affect the firing of the neurons.

Network architecture

A three-layered network was constructed wherein each layer consisted of a 50 x 50 rectangular grid of neurons (Figure 11A). The total synaptic conductance received by a neuron was the sum of gap junction and chemical contributions:

$$I_{syn} = I_{gj} + I_{chem}$$

All neurons in the network were connected to their neighbors by local gap junctional connections. Each neuron was electrically connected to a fraction of the neurons in a rectangular neighborhood of a given size around it. We used a neighborhood of size two, so that each neuron had a total of eight neighbors in its immediate neighborhood, and another 15 in the neighborhood around it. The neuron was randomly connected to half of those neurons j via linear gap junctional connections so that the total contribution to the synaptic current for that neuron i was taken to be

$$I_{gj}^{i} = \sum_{j} g_{gap}(V_i - V_j)$$

We explored several values for the gap junctional connection strength (see Results) and settled on the value of $g_{gap} = 1$ S/cm^2.

In addition to gap junctional connections, the three network layers were also connected by long-range excitatory chemical connections. These connections were bidirectional and between neighboring layers only, so that a neuron from layer 1 received input only from neurons in layer 2, a neuron in layer 3 received input only from neurons in layer 2, while neurons in layer 2 received input from neurons in both layers 1 and 3. The connection probability from one layer to the next was taken to be 5%. The connections were random, so that a neuron in a given layer had an equal probability of being connected to neurons in a neighboring layer. The total contribution to the synaptic current for that neuron i was taken to be

$$I_{chem}^{i} = \sum_{j} g_{chem}(E_{exc} - V_i)$$

where g_{chem} was the maximal excitatory conductance which obeyed first order linear kinetics with a decay time constant of 5 ms. We varied this number and examined the resulting wave properties, using $0.05\,\mu S/cm^2$ for the simulations in Figure 11 and 12. To visualize spiking activity in the two-dimensional grid of neurons in a similar way to calcium imaging in the slice, we convolved the spiking activity for a given cell in space and time. In space, we used a two-dimensional Gaussian filter using a diagonal covariance matrix with standard deviation of 3 cells horizontally and vertically from the chosen cell. In time, we used an exponential filter with a decay time constant of 10 time units. The exact details of this convolution were not important: the spatial convolution helped in visualizing spiking activity of our otherwise point neurons, while the temporal convolution was used to produce longer-lasting activity transients similar to that observed with calcium imaging.

Data analysis

To define waves of synchronous active, we used a threshold of the mean plus four times the standard deviation of the average number of cells active per time step across all three layers. When layers were analyzed individually, a threshold of five was used to define the start points and end points of waves. Statistical significance was calculated using the Student's t-test. An unpaired heteroscedastic test was used to compare model simulations with different parameters. A t-test of the Pearson's correlation coefficient was used where appropriate. All data are presented as mean ± S.E.M.

Results

Modeling a gradient of autonomous activity in a network reproduces key experimental findings.

To determine if the observed differences in cell-autonomous properties between the ventral and dorsal cortices could explain the ventral wave initiation and the directionality of wave propagation towards dorsal areas, we built a network of conductance-based neurons with different cell-autonomous properties. The network consisted of three layers, the first corresponding to the ventral region and the last corresponding to the dorsal region (Fig. 11A). Some fraction of the neurons in each layer was autonomously bursting; to capture the basic differences between the ventral and dorsal cortices, the fraction decreased ventrally to dorsally in agreement with experimental results (see Methods). We investigated the hypothesis that the decreasing gradient of intrinsic excitability is sufficient to generate the directionality of the waves from ventral to dorsal areas.

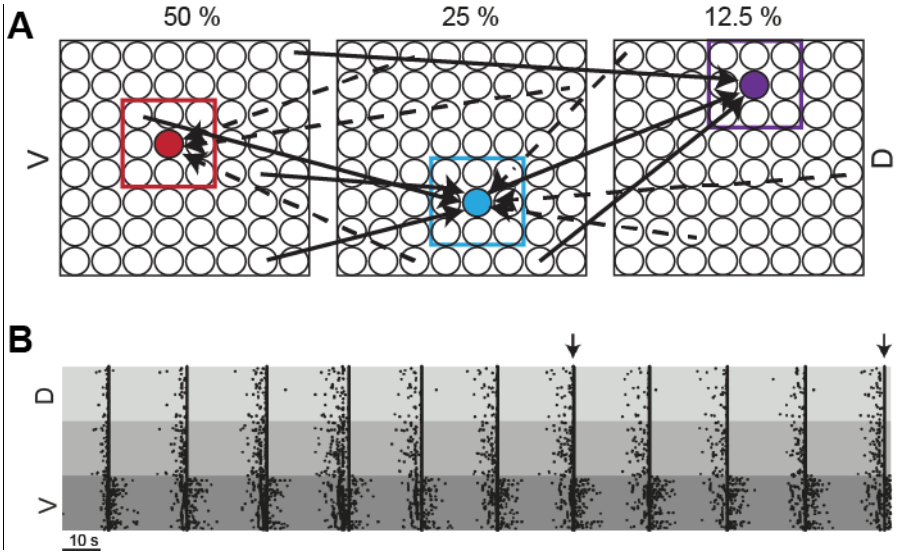

Figure 11. *Network model design and simulation. (A)* Model schematic of three-layered network. Percentages of intrinsically active neurons are displayed at the top of each layer. Colored circles represent neurons whose connections are depicted. Colored boxes represent the gap junctional neighborhood to which each of these cells are connected. Arrows represent synaptic connections between layers. V = ventral; D = dorsal. *(B)* Raster plot of neuronal activity vs. time. Neurons are arranged in vertical layers for each point in time. Black indicates neuronal activity. Waves of synchrony are noted by superimposed vertical

The network was equipped with two kinds of connectivity. To incorporate the experimental findings of the existence of gap junctionally mediated clusters of activity, within each layer, neurons were connected by gap junctions to their nearest neighbors. In the presence

of only local electrical connections, the strength of these connections determined the type of activity generated in the network. Robust waves propagate in the presence of strong local connections (data not shown); however, these waves resemble the waves in the retina and not the cortex. Decreasing the strength of electrical connections creates local clusters of active neurons that propagate in space over a short range and disappear before they reach the edges of the network (data not shown). These local clusters do not propagate across long distances in the network. Because it has been shown experimentally that waves depend on synaptic transmission, these results were not unexpected.

Next, sparse chemical synapses between layers were implemented to establish long-range bidirectional connectivity and generate long-range propagation of activity in the network. Figure 11B shows a network simulation with spontaneously generated wave events. We tuned the adaptation time constant (see Methods) so that waves were generated at frequencies approximating those observed in the experimental system. The two arrows in Figure 11B point to two instances of propagating waves. The raster shown in Figure 12A(left) corresponds to the second arrow. At this time resolution, we observed propagating waves that have clear spatial organization: the waves initiate spontaneously in the first network layer, corresponding to ventral cortical areas, and propagate towards the third layer, corresponding to the dorsal cortex. Since the spike rasters do not capture the spatial organization of wave activity in each layer, we also show a snapshot of the temporal wave dynamics (Fig. 12A, right; Supplemental Movie 3). The spiking activity was convolved over space and time (see Methods) to produce activity similar to that observed with calcium imaging. Here, the black areas denote inactive regions in the network, while white areas denote highly active areas. These time points clearly demonstrate that the initiation of wave activity begins with local clusters in the first network layer, amplified by

local electrical connections, before the activity spreads to layers two and three propagated by the long-range chemical connections. Why does this unidirectional propagation occur despite the presence of bidirectional chemical long-range connections?

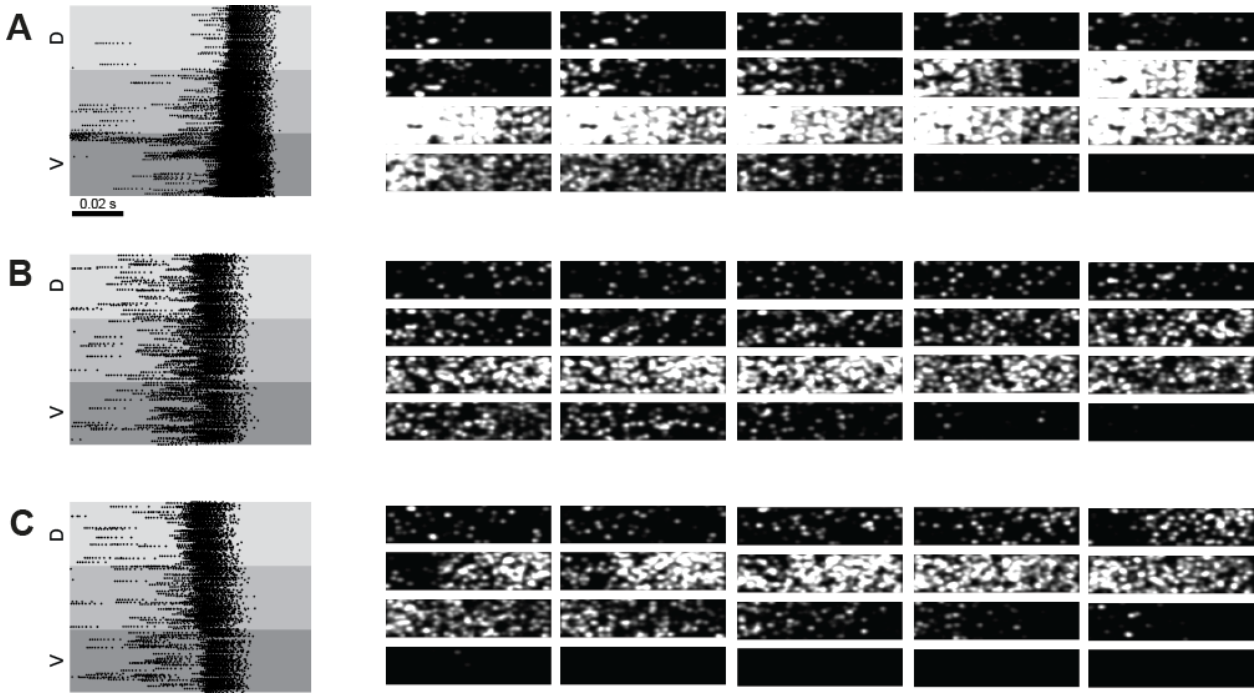

Figure 12. *Examples of waves in different network implementations. (A)* Example wave in a model simulation in which the proportion of intrinsically active cells increased from the dorsal to the ventral layer. Left panel shows a raster of the wave; Right panels show frames from the simulation (see Movie 3). The waves starts in the ventral layer and propagates dorsally. Note that the activity in the ventral layer decays the most slowly. *(B,C)* Example waves in a model simulation with a uniform proportion of intrinsically active cells across the three layers. *(B)* Shows a wave that initiates uniformly across all three layers (Movie 4). *(C)* Shows a wave that initiates in the dorsal layer and propagates ventrally (Movie 5).

We postulated that the reason for this symmetry breaking in the direction of propagation was the imposed gradient of intrinsically bursting cells in the different network layers. Indeed, eliminating this gradient, by giving all layers the same fraction of intrinsically bursting neurons, eliminated the robust unidirectional wave propagation from layer one to three. Figure 12B,C show two example waves generated in a network with a uniform distribution of intrinsically bursting cells across layers. These cells initiate local activity clusters in each layer, hence large-scale activity can initiate anywhere. Figure 12B (Supplemental Movie 4) shows a large-scale

activity that begins in all layers simultaneously, thus there is no directionality of the activity event. In contrast, Figure 12C (Supplemental Movie 5) shows a scenario where a true backward wave is initiated in the third layer, which is then propagated toward the first layer mediated by the long-range synaptic connections.

Model predicts persistence of wave activity near the pacemaker region

One notable feature of wave propagation in the model is that activity not only initiates in the ventral layer, but also persists there at the termination of the wave (see Fig. 12A). That is, the pacemaker region is the first to be active and the last to cease activity. To determine whether this was also a feature of the actual waves, we examined 19 waves that propagated into the dorsal neocortex in 8 P0 slices (E17 + 2DIV). The duration of these waves in the ventral pacemaker, measured from the onset of the macroscopic calcium transient to its 90% decay time was 5.52 $\pm$ 0.5 sec compared to a dorsal wave duration of 2.95 $\pm$ 0.34 sec ($p<0.001$). An example of a propagating wave in which the initiation region shows activity that outlasts the dorsal follower regions is shown in Figure 13A. In some, but not all (5/19), of the waves, the increased duration of activity in the pacemaker region took the form of multiple secondary calcium transients on the falling phase of the primary wave transient. Figure 13B shows plots of calcium transients during wave activity in a slice in which both types of pacemaker activity were observed. The first wave occurs in the left hemisphere and the pacemaker, but not dorsal, wave shows multiple local secondary events. This is followed by a wave in the right hemisphere which shows simple waveforms of activity both ventrally and dorsally. Finally, a second wave occurs in the right hemisphere in which the pacemaker region shows a single secondary transient. These secondary transients were never seen dorsally.

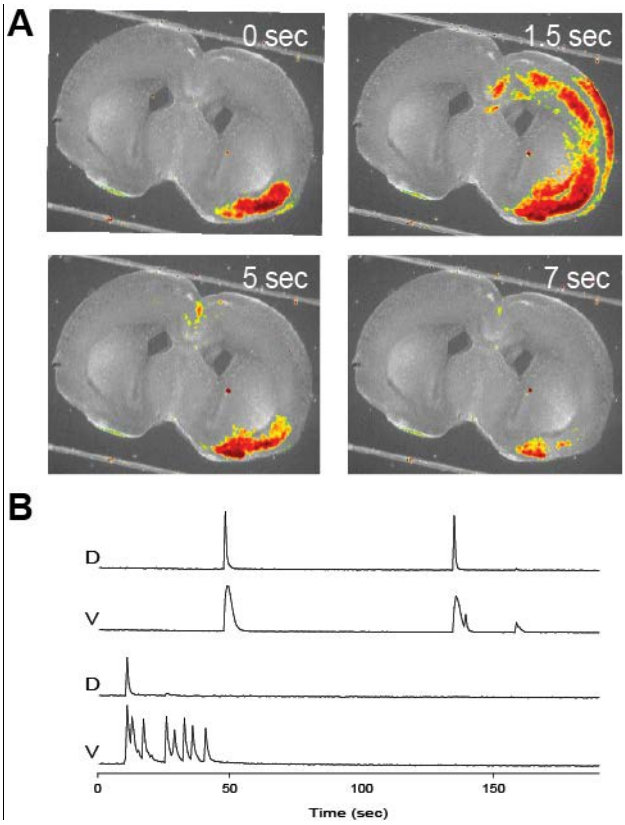

Figure 13. *Persistence of activity in the ventral piriform cortex at the termination of a propagating wave, as predicted by the model* (Fig. 12 A). (A) Montage of images taken during a propagating spontaneous wave in a P0 coronal slice. Activity initiates in the right piriform cortex and propagates throughout the right hemisphere during 1.5 sec. As the wave terminates, activity persists longer in the piriform initiating region than in the dorsal follower regions. (B) Macroscopic calcium transients in ventral and dorsal regions taken from another slice that showed three propagating waves. The first wave, in the right hemisphere (bottom traces) showed repeated after-discharges in the ventral region that were absent in the dorsal region. The second wave occurred in the left hemisphere (top traces), and was associated with a simple ventral calcium transients that was longer in duration than the dorsal transient. The third wave occurred again in the left hemisphere, and the ventral calcium transient was longer than the dorsal transient and showed a single after-discharge on the falling phase.

Proportion of asynchronously active neurons affects wave generation

In order to determine the effect of the proportion of asynchronously active cells on the properties of SSA, we varied the proportion of autonomously active cells in Layer 1, representing the ventral cortex, from 0.20 to 0.50 and observed the behavior of the network. We left all other properties of the network constant. For each simulation, the proportion decreased by 50% from Layer 1 to Layer 2 and then again from Layer 2 to Layer 3 such that, for example, when the proportion in Layer 1 was 0.50, Layer 2 contained 25% autonomously active neurons and Layer 3 contained 12.5%. When the proportion of autonomously active neurons in Layer 1 was 0.20 or 0.25, synchronous waves were not reliably observed although asynchronous activity was present. For simulations with a proportion of at least 0.30 autonomously active neurons,

spontaneously waves of activity were observed. Thus, approximately 30% of neurons must be active in order to generate waves. In simulations with any proportion of autonomously active neurons, all waves propagated from Layer 1 to Layer 3. Therefore, we conclude that the higher level of autonomous activity in the ventral cortex is sufficient to generate waves with a particular directional orientation regardless of the specific proportion of autonomously active cells in layer one. In our experimental studies, the proportion of autonomously active cells was 0.37 ± 0.028 in the ventral cortex and 0.096 ± 0.014 in the dorsal cortex. These numbers would correspond to 0.37 in Layer 1 and 0.096 in Layer 3, parameters which would produce synchronous activity in the model.

The most dramatic effect of varying the proportion of autonomously was observed in the number of cells participating in the wave, which increased significantly as the proportion was raised from 0.30 to 0.50. This trend can be seen in Figure 14A, which the fraction of participating cells for each proportion of autonomously active cells simulated. The correlation coefficient of the linear regression relating these two variables was 0.97 ± 0.15 which was computed using the average fractional participation for each of the five simulations. Thus, there is a significant effect of the proportion of autonomously active cells on the fraction of participating cells ($p < 0.001$, t-test of the Pearson correlation coefficient). The line representing the best linear fit is shown in Figure 14A with a dashed black line. We also analyzed the fractional participation in each layer. The average number of neurons firing during the progression of a wave in a simulation with 50% autonomously active neurons is shown in Figure 14B. Note that the most neurons are active in Layer 1, followed by Layer 2, and that the fewest neurons are active in Layer 3. The number of neurons active in each layer decreased as we

decreased the fraction of active neurons from 0.50 to 0.30, but the relative contributions of each layer to the overall participation did not change.

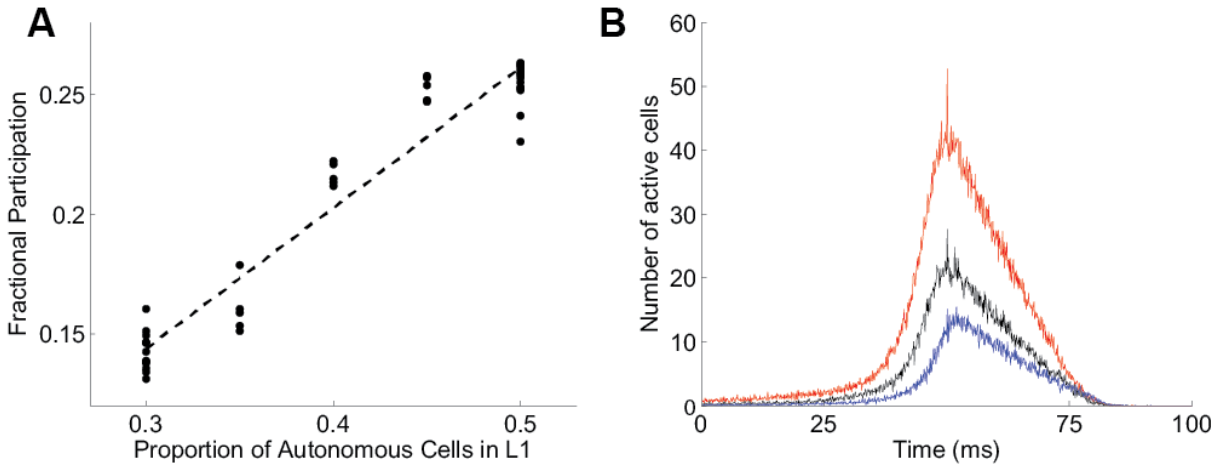

Figure 14. *Participation in waves by layer and proportion of autonomously active cells.(A)* Fraction of participating cells across all three layers vs. the proportion of autonomously active cells in L1. The proportion of autonomously active cells decreased by 50% between layers. Circles show the fraction of participating cells for a single wave during a simulation for a particular parameter value. Dashed line shows the equation of the linear best fit of the data. R^2 = 0.93. *(B)* Number of participating cells by layer for simulations with 50% autonomously active neurons (average of n = 15 waves).

In order to characterize the temporal properties of waves, we analyzed the intervals between waves and the duration of waves as a function of the proportion of autonomously active neurons. Unlike the fraction of participating cells, the relationships between these measures and the parameter we manipulated were not straight forward. The intervals between waves was equivalent for proportions 0.30 and 0.35 as well as for proportions 0.40, 0.45, and 0.50; however, the intervals between waves were slightly but significantly different between these groups. Combining the proportions for which there was no difference in interwave interval, the frequencies of waves were 3.03 ± 0.014 min^{-1} (0.30, 0.35) and 3.17 ± 0.007 min^{-1} (0.40 - 0.50). Although these frequencies were significantly different ($p < 10^{-7}$), the magnitude of the difference was small. In addition, the interwave intervals showed minimal variation with a Fano factor of less than 0.01 for each simulation. These findings indicate that waves in this system

occur at highly regular intervals. The frequency of waves appears to reach a maximum near 40% autonomously active neurons. A limiting factor in the frequency of waves may be the relative refractory period imposed by the conductance g_{sra}.

The duration of waves depended significantly on the proportion of autonomously active cells. Again we observed similar properties for parameter values of 0.30 and 0.35 but differences between these and parameter values of 0.40 - 0.50. For the lower parameter values, the wave duration was quite variable with coefficients of variation 0.25 (83 ± 6.1 ms and 84 ± 9.5 ms, mean ± s.e.m., p = 0.92). As the proportion of autonomously active cells increased, the wave duration increased and its variability decreased. This trend can be seen in Figure 15. The correlation coefficient of the linear regression relating the wave duration to the proportion of asynchronously active cells was 0.75 ± 0.38 (p < 0.001, t-test of the Pearson correlation coefficient). In addition, we investigated the difference in synchrony duration between the three layers. For all five values of the proportion of asynchronously active cells, the wave duration was the longest in Layer 1, followed by Layer 2, and the shortest in Layer 3. The differences between all three layers were significant when compared within any of the five parameter settings. On average, the duration of waves in Layers 2 and 3 was 75 ± 1.5 % and 54 ± 1.8 % of that in Layer 1, respectively. This increased duration in Layer 1 was expected based on the qualitative observations of waves persisting longer in the Layer 1 and in the ventral cortex discussed in the previous section.

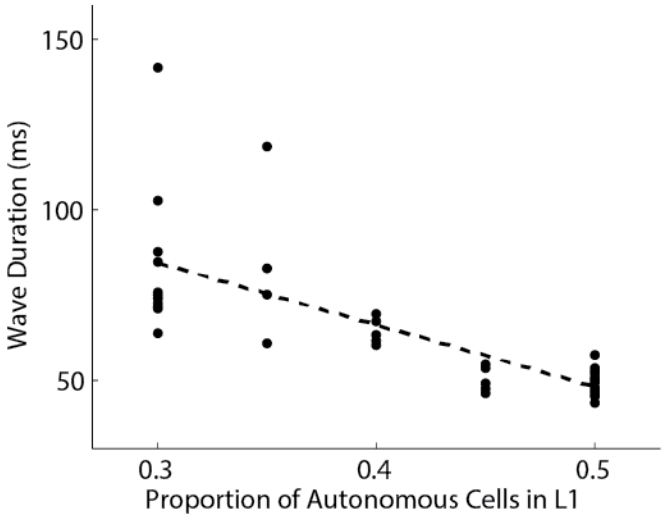

Figure 15. *Duration of waves for different proportions of autonomously active neurons.* The proportion of autonomously active cells decreased by 50% between layers. Circles show the wave duration for a single wave during a simulation for a particular parameter value. Dashed line shows the equation of the linear best fit of the data. $R^2 = 0.56$.

Discussion

The key finding of this computational modeling investigation was that a gradient of autonomously active cells can indeed produce synchronous waves of activity that propagate in one direction. When the number of neurons in the network that could autonomously generate bursting behavior based on their intrinsic cellular properties was at least 30 %, synchronous activity was initiated and propagated. Although the proportion decreased by 50% between layers, waves consistently propagated from the ventral to the dorsal layer, indicating that waves propagate into regions where the amount of autonomous activity is insufficient to independently generate waves. In our experimental data, the ventral cortex contained approximately 37 % autonomously active neurons and the dorsal cortex 9.6 %. Based on the modeling findings, the ventral cortex would be predicted to generate waves while the dorsal cortex would be expected to participate in waves initiating in the ventral cortex but would be unable to independently generate waves. These are exactly the experimental observations we made.

In addition to validating our theory that autonomous activity can induce synchronous waves, the model provided a method for investigating other key questions about the nature of wave generation in autonomously active systems. In this study, we primarily investigated the effect of varying the proportion of autonomously active neurons. Variations of this parameter most notably affected the fraction of neurons that participated in each wave. As we increase the autonomous activity level, the number of neurons participating increased significantly. An number of autonomously active neurons would be predicted to increase the number of cells which would independently generate activity at any given point in time. Since each neuron's activity is amplified by local gap junction connectivity, this may provide the mechanism for the effect observed. The duration of waves decreased slightly reaching a minimum of approximately

50 ms. This duration may be determined by the length of bursts in individual cells, which was approximately 30 ms when cells were autonomously active but were not connected by either gap junctions or chemical synapses. The similarity between these periods suggests that cells are highly correlated during waves, at least in our model system. For relatively low proportions of autonomously active neurons, there was greater variability in the duration of waves. This may reflect an increase in the amount of time necessary for a sufficient number of cells to become active and trigger synchronous activity. In addition, we observed that the as we increased the proportion of autonomously active neurons, the frequency of waves increased slightly and reached a maximum of approximately 3.2 waves/minute. The intervals between waves for all parameter settings were highly regular. These findings suggest that the frequency of waves in our model is set by the time constant τ_{sra} which imposes a relative refractory period on cells after periods of activity.

This model thus validated our hypothesis that autonomous activity in some neurons can produce synchrony in the presence of gap junction and synaptic connectivity. In addition, we should that a gradient of autonomous activity with parameters similar to those found in the experimental system was sufficient to produce directionally oriented waves.

CONCLUSIONS

In this study, we investigated the activity of neurons in the ventral and dorsal neonatal mouse cortex in the periods between large-scale cortical waves in order to gain further insight into the properties that differentiate the two regions. Such differences may explain the spatially asymmetric generation and propagation of SSA, initiating in the ventral (piriform) cortex and propagating dorsally into the neocortex. Two types of activity were observed in the inter-wave period: (1) individual cells produced asynchronous activity and (2) clusters of cells were active in synchronous groups. Individual cells were seen to participate in single-cell asynchronous activity, cluster activity, and synchronous waves, all within a single 5-10 minute imaging period. Wide-field imaging revealed that both types of inter-wave activity were much more common in the ventral compared to the dorsal cortex. We then applied a combination of synaptic antagonists and found that asynchronous cell and cluster activity remained in the absence of synaptic communication. This result indicates that neurons during this period are able to generate activity autonomously and suggests a difference in intrinsic firing properties between ventral and dorsal regions of the cortex. Only $CdCl_2$ was effective in completely eliminating both single cell and cluster activity, indicating that voltage-gated calcium channels are critical in producing such activity. Treatment with octanol eliminated synchronous clusters while preserving single cell activity, suggesting that the propagation of activity within clusters relies on gap junctions.

The higher level of activity during the inter-wave interval in the ventral cortex could provide a mechanism by which the ventral cortex is uniquely able to generate waves. Asynchronous activity generated autonomously by individual neurons and then amplified by gap junctional connectivity may achieve sufficient recruitment of ventral neurons to initiate synchronous waves. To investigate this possibility we constructed a conductance-based network

model with a gradient of cell-autonomous activity that decreased over three layers. We found that this gradient was sufficient to produce directionally propagating waves that replicated key features of experimentally observed SSA. Despite bidirectional synaptic and gap junctional connectivity, waves propagated only from the layer of high autonomous activity towards the layers of lower autonomous activity. Synchronous activity persisted longer in the ventral initiation layer than in the follower layers, recapitulating experimental results. When all layers contained an equal proportion of autonomously active neurons, propagation was not unidirectional and synchrony did not simulate experimental findings. Thus, a gradient of autonomously active cells is necessary and sufficient to produce the type of synchronous activity observed experimentally and is likely to represent a critical feature of the biological network architecture. A second prediction of this model is that during wave propagation, the ventral initiator region will not only be the first to activate, but will be the last region to cease activity at the end of the wave. That is, waves will propagate out of and then recede back into the ventral cortex. Analysis of propagating waves in slices bore out this prediction of the model.

The underlying reason for the increased level of autonomous activity in the piriform is not clear, but the piriform cortex does have several unique features that might explain this phenomenon. The piriform cortex, which in the adult is involved in olfactory processing, is phylogenetically older than the neocortex. The neocortex, which is present only in mammalian species, is characterized by a six-layer organization; in contrast, the piriform cortex is organized in a three-layer morphology and lacks columnar organization. Mature neurons in the piriform cortex have widespread axonal arbors that cover much of the piriform cortex and extend into other cortical areas. Superficial pyramidal (SP) neurons in piriform cortex make a small number of synapses onto a large number of other SP neurons (Johnson et al. 2000). Thus, the piriform

cortex may be particularly well-structured to coordinate activity both within the region itself and across other regions. Indeed, synchronization orchestrated by the piriform cortex has been observed in both physiological and pathological contexts. The region is particularly susceptible to generating epileptiform activity and is believed to play a crucial role in kindling (Loscher and Ebert 1996). Spontaneous rhythmic activity comprised of up- and down-states has also been observed *in vitro* under physiological conditions (Seamari et al. 2007). Developmentally, the paleocortex including the piriform cortex matures slightly earlier than the neocortex. The initiation of SSA may rely on the slightly more mature properties of piriform neurons in contrast to the developmentally younger neurons in the dorsal neocortex. This prediction is in agreement with experiments regarding SSA in the hippocampus which have demonstrated that relatively mature neurons are critical in initiating waves (Picardo et al. 2011).

The clusters of coactive cells we observed appear identical to the domains originally reported by Yuste et al. (1995), in early postnatal rat cortex. They also reported that domain activation was not prevented by TTX and was sensitive to gap junction blockers. The only differences we observed between our clusters and their domains were that we observed almost half of the clusters apparently triggered by 'off' cells, and that in our experiments, we were not able to trigger clusters by temperature drop. We did not study the effects of temperature on clusters in general. In addition to the function of domains in the development of the columnar organization of the cortex, as suggested by Yuste et al., (1995), the present data suggest that they may also play a role in the propagation of spontaneous waves of activity, and thus more generally in activity-dependent development of the cortex.

This study identified significant activity differences between the ventral piriform cortex and the dorsal neocortex during the period between waves. Asynchronously active cells and

active cellular clusters were more prominent in the ventral compared to the dorsal region. To further investigate the implications of these findings, we constructed a computational model to simulate the experimental findings and test our hypothesis that a gradient of autonomously active neurons would produce synchronous wave propagating from areas with a higher concentration to areas with a lower concentration of autonomous active neurons. We used a conductance based model described originally by Baltz et al. (2011) to simulate individual neurons in a three-layer network composed of 50 x 50 grids. Neurons were connected with both gap connections and chemical synapses. This network architecture was supported by our experimental findings which demonstrate that gap junctions are necessary for synchronous activation of small clusters of cells and that synaptic connectivity is necessary for large-scale synchronous waves. We then varied the proportion of autonomously active neurons across the three layers in order to simulate the differences observed between the ventral and dorsal regions. Layer 1 was given the highest proportion of intrinsically bursting neurons and thus represented the ventral cortex while Layer 3 was given the lowest proportion and represented the dorsal cortex.

Using this model, we replicated key experimental findings. Waves were consistently generated in all simulations in which the proportion of autonomously active was at least 0.30, and these waves always propagated from Layer 1 to Layer 3, mimicking the ventral-to-dorsal propagation seen in the experiments. We therefore conclude not only that autonomously active neurons can produce synchronous waves in the absence of external stimuli or synaptic noise but also that a gradient of autonomously active neurons is sufficient to produce directionally oriented waves.

This study presented a unique opportunity to synergistically combine experimental data collection with computational modeling. The experimental findings suggested a theoretical

framework for the initiation and propagation of waves involving both intrinsic cell properties and network structure. Manipulation of either cellular properties or network structure experimentally is challenging to achieve and the interpretation of such experiments may be difficult. Moreover, fine-scale control that allows systematic scaling of parameters cannot be achieved. For example, pharmacological treatment using octanol was used in these studies to block gap junctional connectivity. These experiments demonstrated that gap junctions are likely involved in producing cluster activity; however, experimental modeling could not directly control the strength of gap junctions or the number of cells connected. Modeling studies could be used to answer these more targeted questions. In addition, computational modeling allowed us to investigate questions related to the temporal dynamics of waves that could not be characterized in experimental data due limitations in the precision of imaging acquisition.

Spontaneous synchronous activity in the cortex is unique in that there is a specific region which selectively initiates synchronous while other regions only participate. This stands in contrast to systems such as the retina in which synchrony is generated with approximately equivalent probability throughout the structure. Because of this characteristic topology, we were able to investigate the differing properties in regions which different behavior and make predictions about the origins of such behavior. We were able to test these predictions using a computational model and conclusively demonstrate the ability of a gradient of autonomously active neurons to produce synchronous waves of activity that propagate in a single direction.

REFERENCES

Alléne C, Cattani A, Ackman JB, Bonifazi P, Aniksztejn L, Ben-Ari Y, Cossart R. Sequential generation of two distinct synapse-driven network patterns in developing neocortex. *J Neurosci* 28:12851– 12863, 2006.

Baltz T, de Lima AD, Voigt T. Contribution of GABAergic interneurons to the development of spontaneous activity patterns in cultured neocortical networks. *Front Cell Neurosci* 4:15 eCollection 2010 doi: 10.3389

Baltz T, Herzog A, Voigt T. Slow oscillating population activity in developing cortical networks: models and experimental results. *J Neurophysiol* 106(3): 1500-1514, 2011.

Ben-Ari Y, Cherubini E, Corradetti R, Gaiarsa JL. Giant synaptic potentials in immature rat CA3 hippocampal neurones. *J Physiol* 416: 303-325, 1989.

Cang J, Rentería RC, Kaneko M, Liu X, Copenhagen DR, Stryker MP. Development of precise maps in visual cortex requires patterned spontaneous activity in the retina. *Neuron* 48(5):797-809, 2005.

Conhaim J, Cedarbaum ER, Barahimi M, Moore JG, Becker MI, Gleiss H, Kohl C, Moody WJ. Bimodal septal and cortical triggering and complex propagation patterns of spontaneous waves of activity in the developing mouse cerebral cortex. *Dev Neurobiol* 70(10): 679-692, 2010.

Conhaim J, Easton CR, Becker MI, Barahimi M, Cedarbaum ER, Moore JG, Mather LF, Dabagh S, Minter DJ, Moen SP, Moody WJ. Developmental changes in propagation patterns and transmitter dependence of waves of spontaneous activity in the mouse cerebral cortex. *J Physiol* 589(Pt 10): 2529-2541, 2011.

Corlew R, Bosma MM, Moody WJ. Spontaneous, synchronous electrical activity in neonatal mouse cortical neurones. *J Physiol* 560(Pt 2): 377-390, 2004.

de Lima AD, Opitz T, Voigt T. Irreversible loss of a subpopulation of cortical interneurons in the absence of glutamatergic network activity. *Eur J Neurosci* 19(11): 2931-2943, 2004.

de Lima AD, Lima BD, Voigt T. Earliest spontaneous activity differentially regulates neocortical GABAergic interneuron subpopulations. *Eur J Neurosci* 25(1): 1-16, 2007.

Dzhala V, Valeeva G, Glykys J, Khazipov R, Staley K. Traumatic alterations in GABA signaling disrupt hippocampal network activity in the developing brain. *J. Neurosci.* 32:4017-4031, 2012.

Gust J, Wright JJ, Pratt EB, Bosma MM. Development of synchronized activity of cranial motor neurons in the segmented embryonic mouse hindbrain. *J Physiol* 550(Pt 1): 123-133, 2003.

Huberman AD, Feller MB, Chapman B. Mechanisms underlying development of visual maps and receptive fields. *Ann Rev Neurosci* 31:479–509, 2008.

Johnson DM, Illig KR, Behan M, Haberly LB. New features of connectivity in piriform cortex visualized by intracellular injection of pyramidal cells suggest that "primary" olfactory cortex functions like "association" cortex in other sensory systems. *J Neurosci* 20(18): 6974-6982, 2000.

Kato-Negishi M, Muramoto K, Kawahara M, Kuroda Y, Ichikawa M. Developmental changes of GABAergic synapses formed between primary cultured cortical neurons. *Brain Res Dev Brain Res* 152(2): 99-108, 2004.

Lischalk JW, Easton CR, Moody WJ. Bilaterally propagating waves of spontaneous activity arising from discrete pacemakers in the neonatal mouse cerebral cortex. *Dev Neurobiol* 69(7): 407-414, 2009.

Löscher W, Ebert U. The role of the piriform cortex in kindling. *Prog Neurobiol* 50(5-6): 427-481, 1996.

McCabe AK, Chisholm SL, Picken-Bahrey HL, Moody W.J. The self-regulating nature of **spontaneous** synchronized activity in developing mouse cortical neurones. *J. Physiol.* 577:155-167, 2006.

McCabe AK, Easton CR, Lischalk JW, Moody WJ. Roles of glutamate and GABA receptors in setting the developmental timing of spontaneous synchronized activity in the developing mouse cortex. *Dev Neurobiol* 67(12): 1574-1588, 2007.

Mease RA, Famulare M, Gjorgjieva J, Moody WJ, Fairhall AL. Emergence of adaptive computation by single neurons in the developing cortex. *J Neurosci* 33(30): 12154-12170, 2013.

Meister M, Wong RO, Baylor DA, Shatz CJ. Synchronous bursts of action potentials in ganglion cells of the developing mammalian retina. *Science* 252(5008): 939-943, 1991.

Moody WJ & Bosma MM. Ion channel development, spontaneous activity, and activity-dependent development in nerve and muscle cell. *Physiol Rev* 85(3): 883-941, 2005.

O'Donovan MJ, Wenner P, Chub N, Tabak J, Rinzel J. Mechanisms of spontaneous activity in the developing spinal cord and their relevance to locomotion. *Ann N Y Acad Sci* 860: 130-141, 1998.

Owens DF, Boyce LH, Davis MB, Kriegstein AR. Excitatory GABA responses in embryonic and neonatal cortical slices demonstrated by gramicidin perforated-patch recordings and calcium imaging. *J Neurosci* 16(20): 6414-6423, 1996.

Picardo MA, Guigue P, Bonifazi P, Batista-Brito R, Allene C, Ribas A, Fishell G, Baude A, Cossart R. Pioneer GABA cells comprise a subpopulation of hub neurons in the developing hippocampus. *Neuron* 71(4): 695-709, 2011.

Picken Bahrey HL, Moody WJ. Early development of voltage-gated ion currents and firing properties in neurons of the mouse cerebral cortex. *J Neurophysiol* (4):1761-1773, 2003.

Rivera C, Voipio J, Payne JA, Ruusuvuori E, Lahtinen H, Lamsa K, Pirvola U, Saarma M, Kaila K. The K+/Cl- co-transporter KCC2 renders GABA hyperpolarizing during neuronal maturation. *Nature* 397(6716): 251-255, 1999.

Seamari Y, Narváez JA, Vico FJ, Lobo D, Sanchez-Vives MV. Robust off- and online separation of intracellularly recorded up and down cortical states. *PLoS One* 2(9): e888, 2007.

Shatz CJ, Stryker MP. Prenatal tetrodotoxin infusion blocks segregation of retinogeniculate afferents. *Science* 242(4875): 87-89, 1988.

Smith GD, Cox CL, Sherman SM, Rinzel J. Fourier analysis of sinusoidally driven thalamocortical relay neurons and a minimal integrate-and-fire-or-burst model. *J Neurophysiol* 83(1): 588-610, 2000.

Voigt T, Opitz T, de Lima AD. Activation of early silent synapses by spontaneous synchronous network activity limits the range of neocortical connections. *J Neurosci* 25(18): 4605-15, 2005.